Propagation of uncertainties
in mesocosm experiments on ocean acidification

Dissertation

in fulfillment of the requirements for the degree “Dr. rer. nat”

of the Faculty of Mathematics and Natural Sciences

at Kiel University

submitted by

María Moreno de Castro

Hamburg, 2016

First referee:	Prof. Dr. Kai Wirtz
Second referee:	Prof. Dr. Andreas Oschlies
Date of the oral examination:	29 April 2016
Approved for publication:	30 May 2016
Signed:	Prof. Dr. Wolfgang J. Duschl, Dean

I hereby declare that this work:

a) that apart from the supervisor's guidance the content and design of the thesis is all my own work,

b) the thesis has not already been submitted either partially or wholly as part of a doctoral degree to another examining body and it has not been published or submitted for publication,

c) that the thesis has been prepared subject to the Rules of Good Scientific Practice of the German Research Foundation.

Kiel, 1 March 2016

Maria Moreno de Castro

Contents

Acknowledgments

I would like to express my gratitude to Prof. Dr. Kai Wirtz and Dr. Markus Schartau for giving me the opportunity to start my research in theoretical ecology. Prof. Dr. Hans von Storch, Prof. Dr. Franciscus Colijn and Dr. Dennis Bray provided invaluable scientific comments and support in the critical moments of this thesis. I also thanks Prof. Dr. Andreas Oschlies, Prof. Dr. Inga Hense and Prof. Dr. Martin Wahl, who contributed with their questions and suggestions to definitely improve this monograph.

I also wish to thank my colleagues at Helmholtz-Zentrum of Coastal Research. In particular to Richard, Onur, Jöran and Carsten for their friendship, the amazing scientific discussions and their support in the difficult coding moments. And especially to Changjin, Niousha, Annika, Sabine, Julia, Doris and Wenyan for their warm support in any kind of difficult moments. I thank Ingrid for her charm and advices. Also, thanks to Kaela and Ryan for always bringing freshness (and for their English corrections).

From my research project, I thank Dr. Birte Matthiessen for being a role model for me and I thank Meri for her patience when explaining features, complications and beauty of experimental research in marine biology.

I thank my anchors: Bea, Ana, Jumin, Sonia, Gema and Ruslan, the strongest persons I ever met and my best teachers. I thank Ismael, always there, in his little room in my mind. I thank Juan, who also save me a couple of times. I thank Ricardo, for taking away problems with laughs and free cakes.

Finally, this work could not be done without the encouragement and hope that my mother sends every week, despite the distance, and the passion for maths that my father instilled in me since I was a kid.

Abstract

Beobachtungsdaten von Mesokosmen, die den gleichen experimentellen Bedingungen unterzogen werden, zeigen typischerweise Variabilität. Dies kann die Detektion von Unterschieden zwischen verschiedenen Ansätzen erschweren. Um relevante Quellen der Variabilität zu untersuchen, habe ich eine prozessorientierte, modellbasierte Datenanalyse durchgeführt, in der die Fortpflanzung von Unsicherheiten bercksichtigt wird. Ich beschreibe, wie divergierende Beobachtungsergebnisse innerhalb von Replikaten durch die Amplifikation von Unterschieden von experimentell unberücksichtigten ökologischen Faktoren verursacht werden können. Als Testfälle wurden drei unabhängige Ozeanversauerungs Experimente zur Reaktion von Phytoplankton auf erhöhte CO2 Konzentrationen in aquatischen Systemen herangezogen. Simulationen zur Dynamik der mittleren Phytoplanktonbiomasse für die jeweiligen Ansätze deuten auf einen Versauerungseffekt auf Zeitpunkt und Intensität der Blüte hin ungeachtet der bislang erlangten negativen Ergebnisse mittels statistischer Rükschlussmethoden. Unter Nutzung der mittleren Dynamik konnte ich mittels Modellanalyse zeigen, dass innerhalb der Replikate Unterschiede von Parametern, die sich auf die initiale i) Phytoplanktongemeinschaft und ii) Nährstoffkonzentration beziehen, zu einer höheren Biomassenvariabilität führen, als die Reaktion, die einem Effekt durch erhhte CO2 Konzentrationen zugeschrieben werden kann. Ich konnte Konfidenzintervalle für Parameter und Anfangsbedingungen kalkulieren, die als Toleranz-Schwellwerte dienen können, unter denen initiale experimentelle Unsicherheiten nicht zu hoher Variabilität im Ergebnis fhrt. Diese Information kann die Detektion von Effekten unterschiedlicher Mesokosmos-Ansätze in zukünftigen Experimenten verbessern und trägt zu der laufenden Diskussion über die Interpretation von kontroversen Ergebnissen von Mesokosmos-Experimenten bei.

Observations from different mesocosms exposed to the same treatment typically show variability that hinders the detection of potential treatments effects. To unearth relevant sources of variability, I developed and performed a model-based data analysis that simulates uncertainty propagation. I described how the observed divergence in the outcomes can be due to differences in experimentally unresolved ecological factors within same treatment replicates that get amplified over the course of the experiment. Three independent ocean acidification experiments on the response of phytoplankton to high CO2 concentrations in aquatic environments were used as tests cases. I first simulated the dynamics of the mean phytoplankton biomass in each treatment and detected acidification effects on the timing and intensity of the bloom in spite of the so far negative results obtained by statistical inference tools. By using the mean dynamics as reference for the uncertainty quantification, I showed that differences among replicates in parameters related to initial i) plankton community composition and ii) nutrient concentration can generate higher biomass variability than the response that can be attributed to the effect of elevated levels of CO2. I calculated confidence intervals for parameters and initial conditions. They can serve as estimation of the mesocosms tolerance thresholds below which uncertainties do not escalate into high outcomes variability. This information can improve the detection of treatment effects in next generation experimental designs and contibutes to the ongoing discussion on the interpretation of controversial results in mesocosm experiments.

1

Introduction

Uncertainties in experiments raise the difficulty of providing objective confidence intervals of data. Usually, empirical quantitative information is collected in replicates to ensure uncertainties do not interfere in the detection of the treatment effect. Predicting capabilities of the experiment depend on the statistical similarity of the replicates: replicates are assumed to differ only by fluctuations that are subtle (at least weaker than the expected response to the treatment) and are symmetrically distributed (to vanish in the post-processing average of the outcomes) [Ruxton and Colegrave, 2006].

When uncertainty propagation compromises the similarity of replicates, treatment effects can be masked since unintended slight differences among replicates may escalate and trigger sufficient divergence within a treatment to overweight the variability among treatments. The former variability is usually quantified as the variance of the same treatment replicates and the latter as the variance of the treatment distribution. Popular statistical inference tools essentially make a comparison of these so-called 'variances within and between' treatments [Field et al., 2008]. As statistical inference tools typically take replicates similarity as an axiomatic condition, in experiments with multiple unresolved factors such tools may fail to detect a treatment effect and thereby incur in what it is known as Type II error in hypothesis testing [Field et al., 2008]. This is especially true for low replicate numbers, which drastically reduce the statistical power of the experiment [Cottingham et al., 2005, Peterman, 1990, Miller, 1988].

When uncertainty propagation does not compromise the similarity of replicates it is possible to observe treatment-driven dynamics. In fact, while some uncontrolled

fluctuations may increase over the course of the experiment, raising outcomes variability, other uncertainties are filtered in the system dynamics, allowing for the observation of organized phenomena, such as blooms and extinctions in ecological experiments. The ability to identify what kind of uncertainties get dampened or amplified by the dynamics allow to focus on preventing interventions to enhance the detection of potential responses. Quantitative knowledge of the tolerance thresholds, below which accidental underlaying heterogeneity is not sufficiently strong to mask potential system responses, provides useful information for experimental design and sampling strategies and may help in the interpretation of controversial experimental results. To this end, heuristic constraints to highly-dimensional full-factorial manipulations and the limitations of statistical inference tools promotes the use of dynamical models to investigate which mechanisms regulate uncertainty propagation.

Classical approaches based on model sampling involve testing the robustness of model results to variations of factors controlling the description of the system dynamics, i.e. parameters and initial conditions [Klepper, 1997]. Such analyses are often done point-wise around some reference values of the control factors. Typically, these reference values should be retrieved prior to the sensitivity analysis and should provide a model fit to the experimental or observational data. When replicates are available, model results are fitted to represent the mean of the data. A large sensitivity is revealed if small variations of a factor value induce pronounced changes in model results. In contrast, a low sensitivity is indicated by slightly altered or null changes in modeled outcomes in spite of large variations of a factor value. From a modeling perspective, these sensitivity analyses help to resolve uncertainties in model results.

In this thesis we use a similar approach, although with different objective and interpretation. Our exploration of factor space goes beyond the selection of the best model parametrization and is instead used to simulate outcome variability. The major rationale is to associate the variability in experimental observations to a variational range of each control factor. The confidence interval establishes the limits of the potential values that the uncertainties in the factor can take. In non-intrusive methods of uncertainty quantification, random variations simulating factor uncertainties are included as an additive extension of the deterministic original version of the model. In contrast, intrusive uncertainty propagation occurs when the randomness is multiplicative and entails a coupling between the fluctuations and the dynamics [Toral and Colet,

2014, Chantrasmi and Iaccarino, 2012]. To decompose variability, we simulate how uncertainties propagate through the model to predict the overall variability in the system response. This kind of methods is known as forward propagation of uncertainty, in contrast to backward methods of parameter estimation where the likelihood of inputs values is conditioned by the prior knowledge of the output distribution [Chantrasmi and Iaccarino, 2012, Larssen et al., 2006]. In the following chapters we calculate the confidence intervals of factors for static and time-varying uncertainties and compare results from intrusive and non-intrusive methods.

1.1 Controversial results in phytoplankton mesocosm experiments on ocean acidification

The increase in the global concentration of atmospheric carbon dioxide (CO_2) since the Industrial Revolution is occurring at a rate at least 10 times faster than at any other time in the past 55 million years [Hönisch et al., 2012, Ridgwell et al., 2009]. Oceans are a sink for about 30% of this excess atmospheric CO_2 [Sabine et al., 2004], which increases the carbon dioxide concentration in aquatic environments and alters the balance of carbonate chemistry reactions as: $CO_{2(aq)} + H_2O \leftrightarrow H_2CO_3 \leftrightarrow HCO_3^- + H^+ \leftrightarrow CO_3^{2-} + 2H^+$. The higher the protons concentration, the lower the pH, making the aquatic environment more acidic, a process known as ocean acidification (OA) [Caldeira and Wickett, 2003].

Phytoplankton are responsible for about half of the oxygen and biomass primary production of the planet. They are major contributors to the biological carbon pump, one of the most important global biogeochemical fluxes [Riebesell et al., 2007]. As phytoplankton require CO_2 to perform photosynthesis, their response to acidification can potentially induce climatic feedback [Gattuso et al., 2011]. Moreover, particular attention has been paid to calcifying organisms, such as the coccolithophor *Emiliania huxleyi* (the most abundant phytoplankton species on Earth), as such shell-forming species depend on the saturation state of calcium carbonate in the water, which decreases with increasing CO_2 levels [Kroeker et al., 2013, Riebesell et al., 2000]. However, calcification is positively correlated with HCO_3^- and CO_2 concentrations [Bach et al., 2015]. This illustrates how the sensitivity of the photoautotrophic production to OA is potentially more controversial than previously thought. For instance, a general compilation

of studies on CO_2 enrichment reveals an overall increase in particulate organic matter (POC) [Schluter et al., 2014, Eggers et al., 2014, Zondervan et al., 2001, Riebesell et al., 2000] yet no CO_2 effects in POC abundance [Jones et al., 2014, Engel et al., 2014]. Interestingly, [Jones et al., 2014] found that cells were bigger under higher CO_2 conditions, but the algae grew at lower rates than under present CO_2 conditions. Balanced combinations of both effects can result in no net effect on POC production. Similarly, differences in community composition have also been shown to outweigh OA effects on POC production [Eggers et al., 2014].

High variances are particularly present in mesocosm experiments on phytoplankton responses to OA, even in replicates of the same CO_2 treatment, [Paul et al., 2015, Schulz et al., 2008, Engel et al., 2008, Kim et al., 2006, Engel et al., 2005]. This variability reveals a severe reduction in the ratio between acidification response signal and observation of variability, resulting in a low signal-to-noise ratio. Mesocosms enclose a part of the natural environment under controlled conditions in a suitable compromise between a realistic setting and treatment manageability [Riebesell et al., 2008]. However, mesocosms also contain a higher number of possible interactions, which increases the chances that uncontrolled heterogeneity will spread, compared to batch or chemostat experiments. Moreover, physiological states vary for different phytoplankton cells and environmental conditions, making independent experimental studies prone to divergent results. In addition, it is impracticable to account for every possible factor that occurs in the original environment or to fine-control initial community structure and ecophysiological states between replicates. Incidentally, differences in unresolved details may escalate and produce high standard deviations. Therefore, the identification of the main contributors to the outcome variability is important to ensure reproducibility (thereby a comparison between results of different independent experiments) and to increase the confidence of OA effects on phytoplankton [Broadgate et al., 2013].

Our main working hypotheses on the origins of variability in mesocosms are:

- experimental uncertainties can be interpreted as random variations that compromise the similarity of the biological state among same treatment replicates,

- differences between replicates can be amplified during the experiment and generate considerable divergence within the treatment response,

- the significance of differences can be revealed by the decomposition of outcome variability in terms of the nature, intensity and timing of the amplification.

In this thesis we develop a model-based data-analysis simulating uncertainty propagation. We applied to mesocosm phytoplankton experiments to investigate how the variability observed in experimental outcomes is shaped by unresolved differences in experimental cell physiology and community composition that are not necessarily constant over the course of the experiment and compromise replicates statistical similarity, thus they are reasonably well represented by random variations in model parameters and initial conditions. A possible uncertainty classification is proposed in the next section. It is worth to stress that our analysis provides an estimation of sufficient (but not necessary) causes of controversial results in mesocosm experiments. Other kind of uncertainties that are not considered in this analysis may also contribute to the observed variability.

1.2 Classification of uncertainty in mesocosm experiments

Here we define uncertainties as unresolved details that are difficult, if not impossible, to control or measure during experiments and possibly trigger biomass variability between replicates. Such uncertainties may arise from variations in individual cell physiology or differences in initial bulk biotic and abiotic concentrations in the mesocosms. Uncertainty in mesocosm experiments lack an standard classification. In an attempt to describe here which uncertainties we consider relevant and suitable and which are out of the scope of this thesis, we distinguish here between three types of uncertainties in biomass measurements: fluctuations coming from the medium (external uncertainties), fluctuations inherent to phytoplankton growth (internal uncertainties), and fluctuations due to some unintended dynamics (secondary or side effects).

External uncertainties

External uncertainties are fluctuations that are produced by instrumental or operational bias or by environmental forcing, and that may affect each mesocosm differently, thereby impairing similarity of replicates. By instrumental or operational bias we refer to experimental issues such as handling errors, instrumental precision limitations, perturbations

during sample transport and storage, dissimilarities in the use of standards, or instabilities of the calibration baseline, as much as inaccuracies in data management and reporting. However, the current state-of-the-art of experimental techniques for running plankton mesocosms is so advanced that we believe operational uncertainties to be either of low impact, or well-understood in terms of their consequences for final outcomes [Riebesell et al., 2010, Cornwall and Hurd, 2015]. We do not explicitly focus on this kind of uncertainty in this thesis.

The other kind of external uncertainties is the perturbations from the environmental set-up, like variations in initial abiotic bulk concentrations or fluctuations in photosynthetic available radiation (PAR), temperature, CO_2 aeration, and, in case of outdoor mesocosms, wind or disrupting storms. Theses kinds of uncertainties are suitable for being incorporated into numerical simulations. In this work, we consider uncertainties in initial conditions, in particular, initial nutrient concentration. We do not simulate variations in environmental stressors such as PAR, temperature and CO_2 concentrations, since they are included as inputs taken directly from the measured data.

Internal uncertainties

Internal uncertainties in the phytoplankton response to OA come directly from unresolved details of ecophysiological differences between the assemblages of replicated phytoplankton communities during the filling of the mesocosms. Internal uncertainties are slight changes in the community composition that may, for example, compromise the uniformity of initial fitness status [Kroeker et al., 2013] due to differences in the acclimation history of some dominant populations. This thesis addresses internal uncertainties in detail.

Secondary (side-)effects

It is difficult, if not impossible, to restrict experimental dynamics to the main process of interest. In the case of mesocosm experiments on the phytoplankton response to OA, dynamics not related to the main process can distort mass balance calculations [Riebesell et al., 2008, Egge et al., 2009, Czerny et al., 2013]. Therefore, some secondary or side-effects can remain unresolved. This is the case, for instance, in the presence of

phytoplankton growth or organic matter accumulation at the mesocosm walls, or when organic matter gets lost from the sampled layers via aggregation and sinking. In addition, coagulation of transparent exopolymer particles (TEP) or interactions of the phytoplankton community with microbes or microzooplankton can differ between mesocosms with the same CO_2 treatment. Instead of an explicit and exhaustive description of these (difficult to constrain) processes, we parametrize the loss of biomass via parameters accounting for grazing, sinking of particle aggregates and remineralization.

Model uncertainties

In this thesis we assume two mechanistic descriptions of biomass growth and decay in mesocosm experiments. One model accounts for plankton and detritus dynamics and the other focus in phytoplankton dynamics. Further variations in model characterization including structural variability [Adamson and Morozov, 2014] and uncertainties in model parametrization [Kennedy and O'Hagan, 2001] require extensive analyses which are not considered here.

In the next chapter we describe the models used as reference dynamics for the uncertainty propagation analysis. Then we show how to calculate confidence intervals by implementing static uncertainties within a deterministic model. Later we show our approach for time-varying uncertainties with intrusive and non-intrusive stochastic methods.

2

Reference dynamics

As mentioned in the Introduction, our first hypothesis is that experimental uncertainties can be interpreted as random variations that compromise the similarity of the biological state among same treatment replicates. Here we develop mechanistic models representing the dynamics of such biological state, that is the mean of the replicates of the same treatment. Therefore, we take these descriptions as the reference dynamics for the uncertainty propagation analysis in the next chapters. The model in Section 2.1 describes the reference for static uncertainty propagation in Chapter 3 and the model in Section2.2 describes the reference dynamics for uncertainty propagation in Chapter 4, where we compare static and stochastic approaches.

2.1 Model of particulate organic carbon under acidification conditions

Data integration and dynamics of the state variables

The model simulates the results from the Pelagic Enrichment CO_2 Experiment (PeECE), a set of 9 outdoor mesocosms placed in coastal waters close to Bergen (Norway) during the spring 2003 (PeECE II) and the spring 2005 (PeECE III). In both experiments, blooms of the natural phytoplankton community were induced and treated in three replicates for future, present and past CO_2 conditions [Engel et al., 2008, Schulz et al., 2008, Riebesell et al., 2007, Riebesell et al., 2008]. Experimental data are avail-

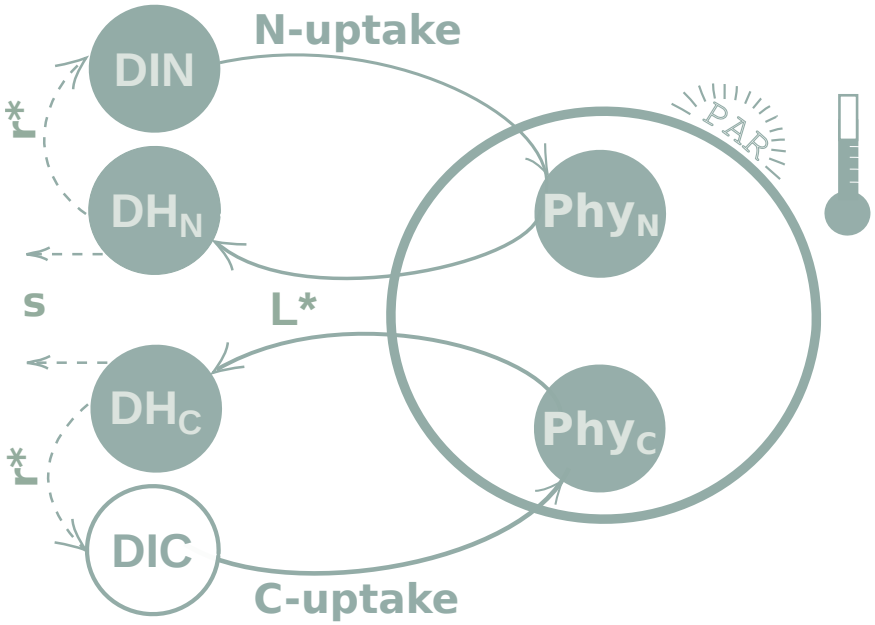

Figure 2.1. Representation of model equations. Dashed lines are fluxes that are only present in the model of POC dynamics (PeECE experiments) but not in the model of phytoplankton dynamics (BIOACID II indoor experiments). DIC, PAR and temperature are the environmental stressors.

able through the data portal Pangaea (doi: 10.1594/PANGAEA.723045 for PeECE II and doi: 10.1594/PANGAEA.726955 for PeECE III). Different species succeeded in the experiments, *Emiliania huxleyi* was the major contributor to POC in PeECE II [Engel et al., 2008] but also diatoms significantly bloomed during PeECE III [Schulz et al., 2008]. The same parameter set is applied for both experiments as is given in Table 2.1. Field data of aquatic CO_2 concentration, temperature and light, were taken as direct model inputs (Fig. A.2). Measurements of phytoplankton abundance, biomass or species composition were controversial. Instead, POC, PON and DIN serve for model calibration. POC and PON data were adjusted for a direct comparison with model results (see SectionA.3), since some contributions to POC remain unresolved by our dynamical equations. In fact, state variables of our model comprise carbon and nitrogen content of phytoplankton, $\mathrm{Phy_C}$ and $\mathrm{Phy_N}$ and dissolved inorganic nitrogen, DIN, as representative for all nutrients. The dynamics of non phytoplanktonic components DH, i.e. detritus and heterotrophs, are distinguished by $\mathrm{DH_C}$ and $\mathrm{DH_N}$, such as POC = $\mathrm{Phy_C} + \mathrm{DH_C}$ and PON = $\mathrm{Phy_N} + \mathrm{DH_N}$. Then, the dynamics of the state variables for PeECE model

is given by

$$\frac{\mathrm{dPhy_C}}{\mathrm{dt}} = (\mathrm{P\text{-}R\text{-}L}) \cdot \mathrm{Phy_C} \tag{2.1}$$

$$\frac{\mathrm{dPhy_N}}{\mathrm{dt}} = \mathrm{V} \cdot \mathrm{Phy_C} - \mathrm{L} \cdot \mathrm{Phy_N} \tag{2.2}$$

$$\frac{\mathrm{dDIN}}{\mathrm{dt}} = \mathrm{r} \cdot \mathrm{DH_N} - \mathrm{V} \cdot \mathrm{Phy_C} \tag{2.3}$$

$$\frac{\mathrm{dDH_C}}{\mathrm{dt}} = \mathrm{L} \cdot \mathrm{Phy_C} - (\mathrm{s} \cdot \mathrm{DH_C} + \mathrm{r}) \cdot \mathrm{DH_C} \tag{2.4}$$

$$\frac{\mathrm{dDH_N}}{\mathrm{dt}} = \mathrm{L} \cdot \mathrm{Phy_N} - (\mathrm{s} \cdot \mathrm{DH_N} + \mathrm{r}) \cdot \mathrm{DH_N} \tag{2.5}$$

Initial conditions are estimated from experimental data as $\mathrm{Phy_C}(0) = 2.5\mu\mathrm{mol\text{-}C\,L^{-1}}$, $\mathrm{Phy_N}(0) = 0.4\mu\mathrm{mol\text{-}N\,L^{-1}}$ and DIN$= 8\mu$mol-N L^{-1} for PeECE II and DIN$= 14\mu$mol-N L^{-1} for PeECE III.

Primary production and respiratory terms are described in 2.3. Loss rate of phytoplankton biomass is a density dependent term

$$\mathrm{L} = \mathrm{L^*} \cdot (\mathrm{Phy_C} + \mathrm{DH_C}).$$

The resulting matter flux increases the biomass of detritus and heterotrophs (DH) and a fraction of it becomes part of the remineralizable pool. A temperature dependent remineralization term [Schartau et al., 2007]

$$\mathrm{r} = \mathrm{r^*} \cdot \mathrm{f_T}$$

describes any kind of DIN production, as hydrolysis and remineralization of organic matter, excretion of ammonia directly by zooplankton and rapid remineralization of fecal pellets produced also by zooplankton. The other fraction of the non phytoplanktonic biomass is removed by settling with a rate related to the sinking coefficient, s, given in Eqs. 2.1 and 2.1. Our model is calibrated with experimental data from enclosed mesocosms where aquarium pumps ensured mixing. Therefore we assume that wealthy enough organisms were able to achieve neutral buoyancy [Boyd and Gradmann, 2002] thus sinking does not directly affect phytoplankton biomass.

The CO_2 effect on POC dynamics

This model reproduces the mean of PON, POC and DIN experimental data per treatment (Fig. 2.4). For PeECE II, PON is moderately overestimated and postbloom POC

Table 2.1. Parameter values used for the reference run of PeECE experimental data. All values are common to both PeECE II and III experiments, only the mean temperature (determined by environmental forcing) and the averaged cell size in the community are different.

Parameter		Value	Units	State Variable	Reference
a_{CO2}	carbon acquisition	0.15	$(\mu$mol-C $)^{-1}$L	Phy_C	this study
a_{PAR}	light absorption	0.7	μmol phot $^{-1}$m^{2}s	”	[Wirtz, 2013]
a^*	C-acquis. coeff.	0.15	μm^{-1}	”	this study
P_{max}	max. photosyn. rate	12	d^{-1}	”	this study
Q^*_{subs}	subsist. quota offset	0.33	mol-N (mol-C)$^{-1}$	”	this study
α_Q	Q_{subs} allometry	0.4	-	”	this study
ζ	costs of N assimil.	2	mol-C (mol-N)$^{-1}$	”	[Raven, 1980]
ℓ	size Ln(ESD/1μm)	1.6	-	Phy_C, Phy_N, DIN	PeECE II data
		1.8	-		PeECE III data
f_p	fraction of protein photo. machinery	0.4	-	”	this study
V^*_{max}	max. nutrient uptake	0.5	mol-N (mol-C d)$^{-1}$	”	this study
Aff	nutrient affinity	0.2	$(\mu$mol-C d$)^{-1}$L	”	this study
α_V	V_{max} allometry	0.45	-	”	[Edwards et al., 2012]
L^*	phyto. losses coeff.	$11 \cdot 10^{-3}$	$(\mu$mol-C d$)^{-1}$	Phy_C, Phy_N and , DH_C, DH_N	this study
r^*	DIN remin. & excret.	1.5	d^{-1}	DH_C, DH_N	this study
s	DH sinking	10	L$(\mu$mol-C d$)^{-1}$	”	this study
T_{ref}	referen. temperature	8.3	Celsius	Phy_C, Phy_N and	PeECE II data
		10.1	Celsius	DIN, DH_C, DH_N	PeECE III data

is slightly underestimated. Even so, the model fits the experimental data with similar precision than the treatment mean of the experimental data (see Table A.1). Treatment means and their associated standard deviations are typically used to describe experimental data (see Fig. 1b in [Engel et al., 2008] for PeECE II or Fig. 8a in [Schulz et al., 2008] for PeECE III) and are the foundations of statistical inference tools, which did not detect acidification responses for PeECE II and III. However, with our mechanistic model-based analysis, POC time series under future CO_2 conditions suggests an earlier and elevated bloom with respect to past CO_2 conditions (Fig. 2.3).

2.2 Model of phytoplankton under acidification and warming conditions

Data integration and dynamics of the state variables

A simplification of the previous model represents the reference dynamics of phytoplankton growth and decay by the temporal evolution of the state variables carbon and nitrogen content of phytoplankton, $\mathrm{Phy_C}$ and $\mathrm{Phy_N}$ and dissolved inorganic nitrogen, DIN

$$\begin{aligned} \frac{\mathrm{dPhy_C}}{\mathrm{dt}} &= (\mathrm{P\text{-}R\text{-}L}) \cdot \mathrm{Phy_C} \\ \frac{\mathrm{dPhy_N}}{\mathrm{dt}} &= \mathrm{V} \cdot \mathrm{Phy_C} - \mathrm{L} \cdot \mathrm{Phy_N} \\ \frac{\mathrm{dDIN}}{\mathrm{dt}} &= -\mathrm{V} \cdot \mathrm{Phy_C}. \end{aligned} \tag{2.6}$$

This model is calibrated with phytoplankton abundance data (we lack this information for the model shown in the previous Section) from the indoor mesocosm experiments with plankton autumn communities of Kiel fjord (Germany) in 2012 (doi.10.1594/PANGAEA.840852 for BIOACID II), a factorial set-up at high and low CO_2 conditions and 9 and 15 Celsius temperatures. Phytoplankton bloom consisted mainly in diatoms. Environmental forcings showed in Fig. A.2 are implemented as model inputs. Initial conditions are estimated from experimental data as $\mathrm{Phy_C}(0) = 1\mu\mathrm{mol\text{-}C\,L^{-1}}$, $\mathrm{Phy_N}(0) = 0.1\mu\mathrm{mol\text{-}N\,L^{-1}}$ and DIN$= 10\mu\mathrm{mol\text{-}N\,L^{-1}}$.

Primary production and respiratory terms are described in Section 2.3. We assume grazing is the main cause of phytoplankton biomass removal as suggested by [Paul et al., 2015]. A relationship between an increase in their production and an increase in

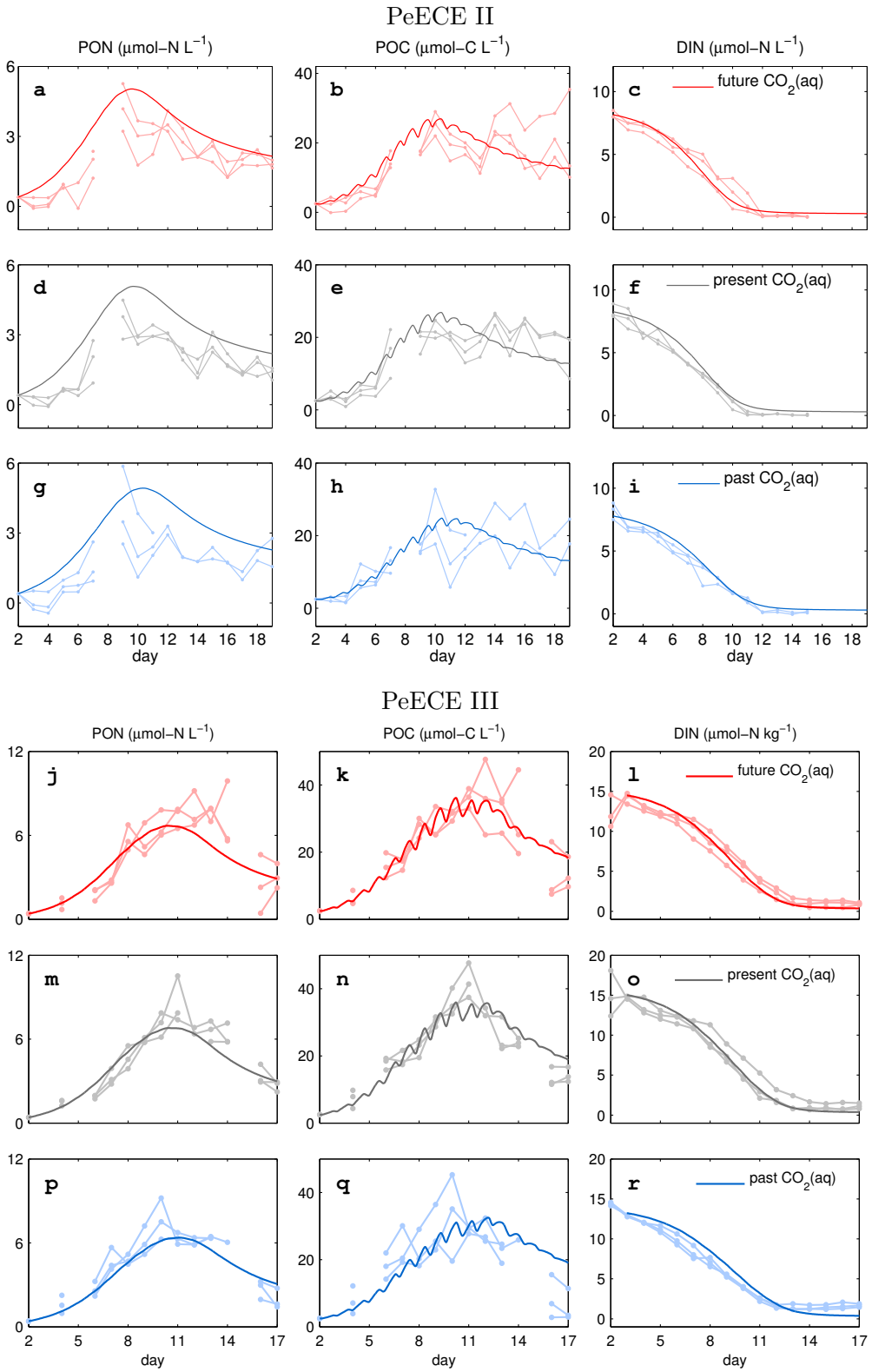

Figure 2.2. Reference runs for POC, PON and DIN simulating the mean of the replicates per treatment are in solid lines, with different colors for the three experimental CO_2 set-ups. Dots are three times replicated data from the Pelagic Enrichment CO_2 Experiment (PeECE II and III).

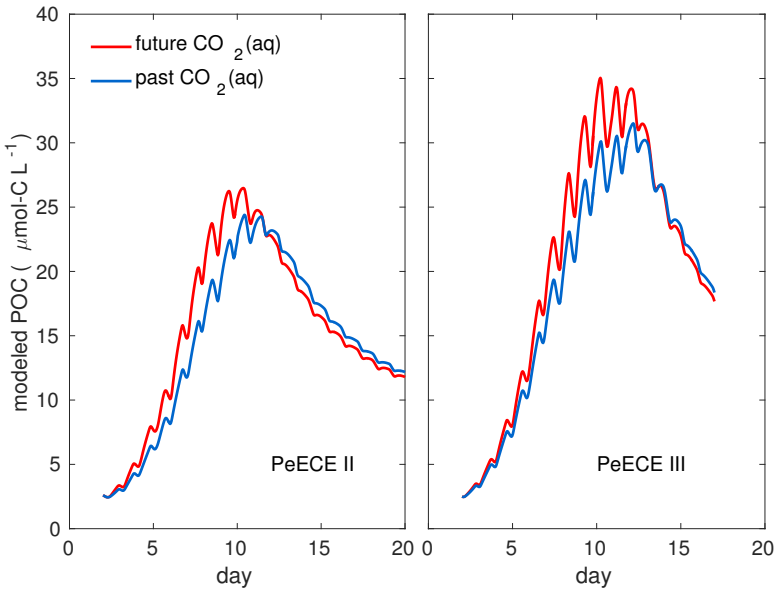

Figure 2.3. Reference simulations of POC for high CO_2 (red) and low CO_2 (blue) experimental conditions show and earlier and more intense bloom under acidification conditions.

temperature has often been observed [Weisse and Montagnes, ,Montagnes and Lessard, 1999, Rose, 2007], then phytoplankton biomass losses, L, are temperature dependent. Therefore zooplankton effect is parametrized as $L = L^* \cdot f_T^{zoo}$ with f_T^{zoo} described by the Arrhenius equation for protein folding as in Eq. 2.8. Parameters are given in Table 2.2

Warming and CO_2 effects on phytoplankton dynamics

Our model for BIOACID II data reproduces the mean of phytoplankton and nutrients dynamics. Reference runs are shown in Fig. 2.4. Phytoplankton carbon is moderately overestimated for the treatment with high temperatures and low acidification, while underestimated for the cold treatments. Even so, the model fits the experimental data with similar precision than the treatment mean of the experimental data (see Table A.1). With our mechanistic model-based analysis, phytoplankton growth in acidified environment shows an earlier and elevated bloom with respect to past CO_2 conditions (see Fig. 2.5) as showed for POC in the previous model. About temperature, our model reproduces the effect reported in [Paul et al., 2015], i.e. a phytoplankton carbon Phy_C decreases by more than half with increasing temperature at bloom time. Synergistic effects of warming and acidification in phytoplankton biomass were not detected by sta-

Table 2.2. Parameter values used for the reference run of BIOACID II indoor mesocosms data. Due to linearity constrains specific to our method, only uncertainties in parameters in bold are explored with .

	Parameter	Value	Units	State Variable	Reference
a_{CO2}	carbon acquisition	0.15	$(\mu\text{mol-C})^{-1}\text{L}$	Phy_C	this study
a_{PAR}	light absorption	0.7	$\mu\text{mol phot}^{-1}\text{m}^2\text{s}$	”	[Wirtz, 2013]
a^*	C-acquis. coeff.	0.15	μm^{-1}	”	this study
$\mathbf{P_{max}}$	**max. photosyn. rate**	**12**	$\mathbf{d^{-1}}$	**”**	**this study**
$\mathbf{Q^*_{subs}}$	**subsist. quota offset**	**0.33**	$\mathbf{mol\text{-}N\,(mol\text{-}C)^{-1}}$	**”**	**this study**
α_Q	Q_{subs} allometry	0.4	-	”	this study
ζ	costs of N assimil.	2	$\text{mol-C}\,(\text{mol-N})^{-1}$	”	[Raven, 1980]
ℓ	size Ln(ESD/1μm)	1.5	-	Phy_C, Phy_N, DIN	BIOACID II data
$\mathbf{f_p}$	**fraction of protein for photosynthesis**	**0.4**	**-**	**”**	**this study**
V^*_{max}	max. nutrients uptake	0.5	$\text{mol-N}\,(\text{mol-C}\,\text{d})^{-1}$	”	this study
Aff	nutrient affinity	0.2	$(\mu\text{mol-C}\,\text{d})^{-1}\text{L}$	”	this study
α_V	V_{max} allometry	0.45	-	”	[Edwards et al., 2012]
$\mathbf{L^*}$	**phyto. losses coeff.**	$11 \cdot 10^{-3}$	$\mathbf{(\mu mol\text{-}C\,d)^{-1}}$	$\mathbf{Phy_C}$, $\mathbf{Phy_N}$	**this study**
T_{ref}	referen. temperature	9	Celsius	Phy_C, Phy_N, DIN	BIOACID II data

tistical inference tools described in [Paul et al., 2015]. With our mechanistic description for the reference dynamics per treatments we observe that acidification effects on bloom intensity are amplified at low temperatures, revealing acidification and warming may have antagonistic effects on plankton communities.

2.3 Definition of relative growth rate

Relative growth rate μ is calculated from primary production rate subtracting respiration and mortality losses, $\mu = \text{P} - \text{R} - \text{L}$. Mortality losses were already described in previous sections, thus we develop here the representation of P and R.

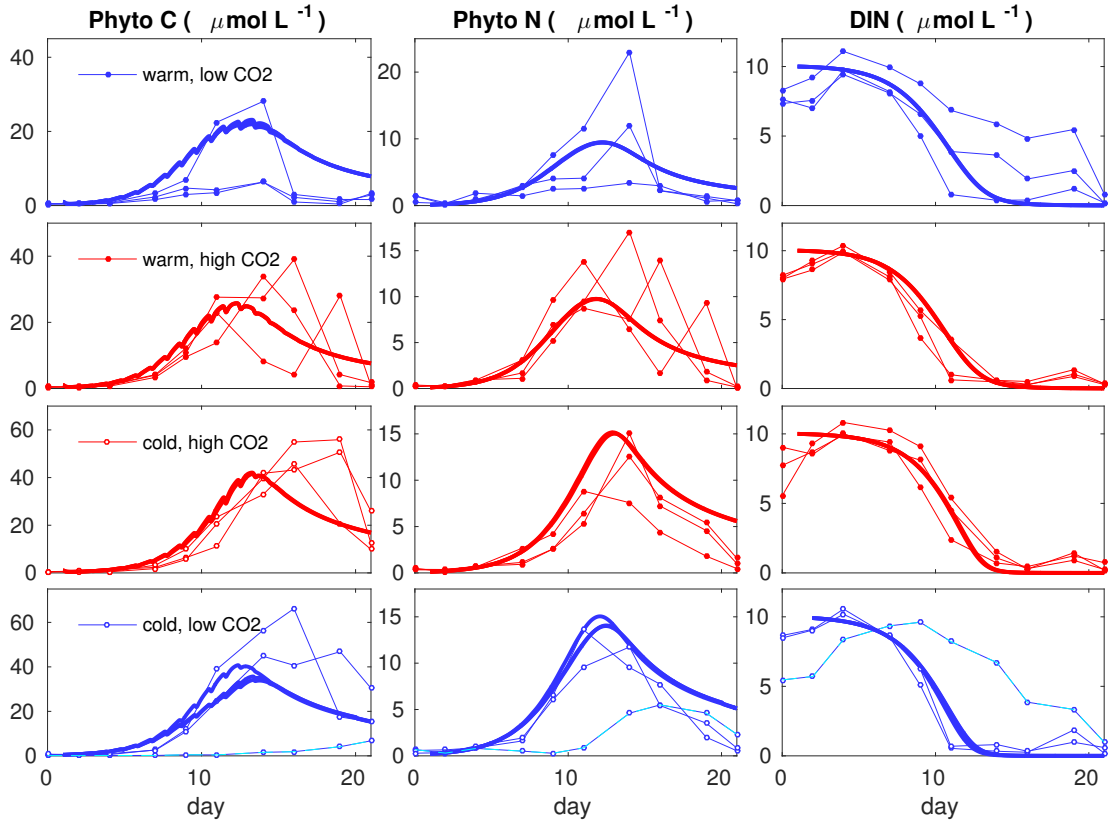

Figure 2.4. Model reference runs for phytoplankton biomass reproducing the mean of the replicates per treatment are in solid lines, with different legend for the temperature (warm and cold) and CO_2 (high and low) treatments. CO_2 measurements were collected per mesocosm and those data are taken as model inputs (see Fig. A.2), which produce different model solutions per replicate (only visible for the treatment in the last raw). Dots are three times replicated data from BIOACID II indoor mesocosm experiments. Aberrant trajectory in the last row shows a malfunctioned replicate that we exclude of our analysis, following [Sommer et al., 2015].

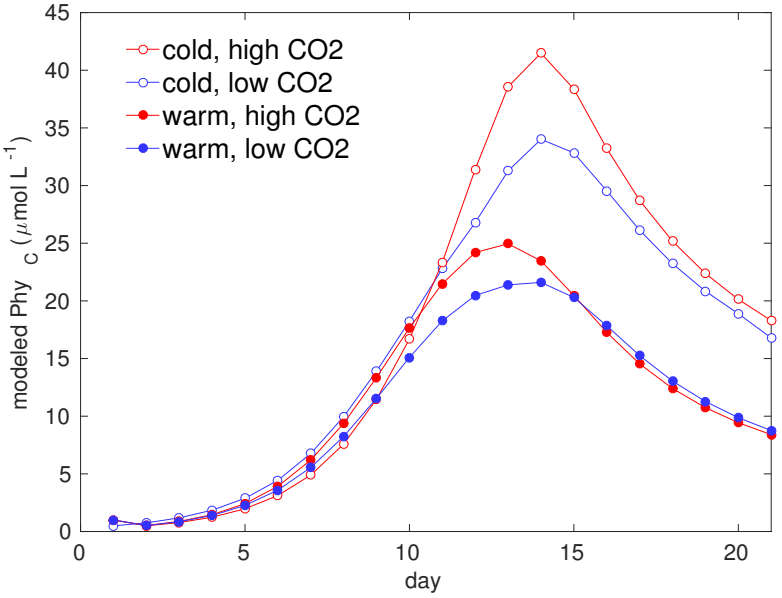

Figure 2.5. Comparison of model reference runs for phytoplankton biomass reproducing the mean of the replicates per treatment. Model projections show that warming and acidification affects bloom intensity and timing.

Primary production

Primary production rate reflects the limiting effects of light, dissolved inorganic carbon (DIC), temperature and nutrient internal quota,

$$\mathrm{P} = \mathrm{P_{max}} \cdot \mathrm{f_{PAR}} \cdot \mathrm{f_{CO2}} \cdot \mathrm{f_T} \cdot \mathrm{f_Q} \cdot \mathrm{f}_p. \tag{2.7}$$

$\mathrm{P_{max}}$ is the maximum primary production rate. Specific light $\mathrm{f_{PAR}}$ depends on light and DIC. PAR for the indoor mesocosm experiment was provided by lamps. For outdoor experiments, we calculate the attenuation coefficient, a_z, considering that in coastal regions light intensity is reduced to 1% of its surface value typically in 5 m [Denman and Gargett, 1983] and that about 80% of the incident light passes through the mesocosm upper cover [Schulz et al., 2008]. We obtain $\mathrm{a}_z = 0.75\mathrm{m}^{-1}$. Then, spatially averaged PAR experienced by cells at mixed layer depth (MLD= $4.5\,m$, [Engel et al., 2008]), is calculated from radiation at water surface, PAR_0 (shown in Fig. A.2), following an exponential decay described by the Lambert-Beer law

$$\langle \mathrm{PAR} \rangle_z = \frac{\mathrm{PAR}_0}{ML} \int_0^{MLD} e^{-\mathrm{a}_z \cdot z} dz.$$

The relationship between photosynthesis and irradiance can be formulated referring to a cumulative one-hit Poisson distribution [Ley and Mauzerall, 1982,Dubinsky et al., 1986]. With the temperature and carbon acquisition dependence, it yields

$$\mathrm{f_{PAR}} = \left(1 - e^{-\frac{\mathrm{a_{PAR}} \cdot \langle \mathrm{PAR} \rangle_z}{\mathrm{P_{max}} \cdot \mathrm{f_{CO2}} \cdot \mathrm{f_T}}}\right),$$

where $\mathrm{a_{PAR}}$ is the effective absorption related to the chloroplast cross-section and saturation response time for receptors [Geider et al., 1998a, Wirtz and Pahlow, 2010], the carbon acquisition term $\mathrm{f_{CO2}}$, Eq. 2.9. $\mathrm{f_T}$ is the temperature dependence. We consider that all metabolic rates depend on protein folding that increases with rising temperature following the Arrhenius equation [Scalley and Baker, 1997] as described in [Geider et al., 1998b] or [Schartau et al., 2007]

$$\mathrm{f_T} = e^{-\mathrm{E_a} \cdot \left(\frac{1}{\mathrm{T}} - \frac{1}{\mathrm{T_{ref}}}\right)}, \tag{2.8}$$

with activation energy $\mathrm{E_a} = \frac{\mathrm{T_{ref}^2}}{10} \cdot log(Q_{10})$ as in [Wirtz, 2013], and $\mathrm{T_{ref}}$ is the mean measured temperature (see Fig. A.2). For PeECE experiments we take $Q_{10} = 1.88$ for phytoplankton [Eppley, 1972, Brush et al., 2002]. In the indoor experiments, we use $Q_{10} = 1.48$ for diatoms [Suzuki and Takahashi, 1995]. For zooplankton, a higher value, $Q_{10} = 2.5$, represents enhanced metabolism under warming conditions.

According to [Peters, 1983, Brown et al., 1995, Bonner, 2006], among others, size is a driving force for all of biology because it determines important biological features as strength, surface area, complexity, rate of metabolism, organism abundance, turn over or life span. About phytoplankton, several studies unearthed the importance of size to describe metabolic rates [Peters, 1983,Marbà et al., 2007]. In particular, recent empirical and theoretical studies described the relation of phytoplankton size with subsistence quota, light acquisition or nutrient and carbon uptake by allometric relations [Litchman and Klausmeier, 2008,Litchman et al., 2009,Wirtz, 2011], as well as how size-dependences scale from cellular to ecosystem level [Litchman et al., 2007, Litchman et al., 2010]. Taking this into account, the mean cell size in the community is a suitable way to include species composition and size structure in marine ecosystem models, which is relevant since we aim to investigate how much uncertainties in community composition among replicates may escalate into high variability within a treatment. Here the mean cell size in the community is represented as the logarithm of the mean equivalent spherical diameter ESD, $\ell = Ln(ESD/1\mu m)$.

To resolve sensitivities to different DIC conditions, we seek for a relatively accurate description of carbon acquisition as a function of DIC and size. It has been suggested by previous observations and models that ambient DIC concentration increases primary production [Schluter et al., 2014, Rost et al., 2003, Zondervan et al., 2001, Riebesell et al., 2000, Chen, 1994, Riebesell et al., 1993] and mean cell size in the community [Sommer et al., 2015, Eggers et al., 2014, Tortell et al., 2008]. We adopted and simplified a biophysically explicit description for carbon uptake from [Wirtz, 2011], where the efficiency of intracellular DIC transport has been derived as a function of mean cell size and CO_2 concentration. For very large cells, the formulation converges to the surface to volume ratio, that in our notation reads $e^{-\ell}$. By contrast, the allometric dependence of primary production on CO_2 does not apply to picophytoplankton so that together we have a non-uniform allometric scaling $\mathrm{f_{CO2}}(\ell)$ in the carboxylation rate

$$\mathrm{f_{CO2}} = \Big(\frac{1 - e^{-\mathrm{a_{CO2}}\cdot \mathrm{CO_2}}}{1 + \mathrm{a^*} \cdot e^{(\ell - \mathrm{a_{CO2}}\cdot \mathrm{CO_2})}}\Big). \tag{2.9}$$

The specific carbon absorption coefficient $\mathrm{a_{CO2}}$ reflects size-independent features of the DIC acquisition machinery, such as carbon concentration mechanisms [Raven and Beardall, 2003].

The allometric factor α_Q quantifies the scaling relation of subsistence quota and cell size. We use a Droop dependency on nutrient N:C ratio [Droop, 1973] which has been recently mechanistically derived [Wirtz and Pahlow, 2010, Pahlow and Oschlies, 2013]

$$\mathrm{f_Q} = \Big(1 - \frac{\mathrm{Q_{subs}}}{Q}\Big)$$

where $Q = \frac{\mathrm{Phy_N}}{\mathrm{Phy_C}}$. Its lower reference, the subsistence quota $\mathrm{Q_{subs}} = \mathrm{Q^*_{subs}} \cdot e^{-\alpha_Q \cdot \ell}$, is considered size dependent to reflect a lower protein demand for uptake mechanisms in large cells [Litchman et al., 2007].

The last term in Eq. 2.7 accounts for an energy allocation trade-off in phytoplankton cells: protein allocation for photosynthetic compounds as RuBisCo and pigments, $\mathrm{f_p}$, versus allocation for nutrient uptake, $\mathrm{f_v}$, expressed by $\mathrm{f_p} + \mathrm{f_v} = 1$. Since we are concerned about variability reconstruction rather than in the most accurate description, for instance, based on optimal allocation [Wirtz and Pahlow, 2010, Pahlow and Oschlies, 2013], we favored a simplify detailed partition models by setting the trait fractions constant. In stead of describing trait variations, we describe trade-offs in steady state in

terms of size and energy allocation, for constraining the parametrization during the calibration process. The explicit account for trade-off steps towards a more mechanistic description of the growth rate.

Respiratory cost and nutrient uptake rates

Efforts related to nutrient uptake V are represented by a respiration term because basic maintenance respiration expenses are neglected [Wirtz and Pahlow, 2010]. Respiration rate is then calculated as

$$\mathrm{R} = \zeta \cdot V$$

where ζ expresses the specific respiratory cost of nitrogen assimilation [Raven, 1980, Aksnes and Egge, 1991, Geider et al., 1998b, Pahlow, 2005]. For simplicity, our model merges the set of potentially limiting nutrients (e.g. P, Si and N) to a single resource only, that is DIN. We follow [Aksnes and Egge, 1991] as described in [Pahlow, 2005] for the maximum uptake rate

$$\mathrm{V_{max}} = \frac{1}{\frac{1}{\mathrm{V^*_{max}} \cdot \mathrm{f_T}} + \frac{1}{\mathrm{Aff} \cdot \mathrm{DIN}}},$$

comprising the maximum uptake coefficient, $\mathrm{V^*_{max}}$, and the nutrient affinity, Aff. Besides adding a temperature dependence of nutrient uptake as given in [Schartau et al., 2007], we assume that respiratory costs decrease with increasing cell size [Edwards et al., 2012] which leads to an allometric scaling in nutrient uptake [Wirtz, 2013] with exponent α_V. We also account for the static proteins allocation trade-off between photosynthetic machinery, $\mathrm{f_p}$, and nutrients uptake, $\mathrm{f_v} = 1 - \mathrm{f_p}$. Then the nutrient uptake term is

$$V = (1 - \mathrm{f_p}) \cdot \mathrm{V_{max}} \cdot e^{-\alpha_V \cdot \ell}.$$

3

Propagation of static uncertainties

3.1 Method

In this chapter we perform an uncertainty propagation analysis with the reference dynamics described in Section 2.1. Variability induced by uncertainties simulated as variations of the model control factors is compared with the variability in POC experimental data. The comparison between simulated and experimental variability in POC helps us to identify those changes in physiological state and in community structure that are main potential contributors to the variability.

We consider 19 model factors, ϕ_i, with $i = 1, ..., N = 19$, made of 14 process parameters and 5 initial conditions for the state variables in Eqs. 2.1. In Table 2.1 we show the reference values, $\langle\phi_i\rangle$, where brackets denote ensemble average. Factor variations are introduced as random values within the variational range $[\langle\phi_i\rangle - \triangle\phi_i, \langle\phi_i\rangle + \triangle\phi_i]$, where $\triangle\phi_i$ is the standard deviation of the normal distribution of possible factor values. To calculate $\triangle\phi_i$, we first generate 10^4 simulations, each one with a different factor value, ϕ_i. The ensemble of model solutions represents possible replicate realizations (see Fig. 3.1). The factor value for each POC trajectory is randomly drawn from a normal distribution around the factor reference value $\langle\phi_i\rangle$, which is the residual distribution assumed by parametric statistical inference tools as ANOVA [Field et al., 2008]. We take the ensemble average over modeled replicates and calculate the standard deviation, $\triangle\mathrm{POC}_i^{\mathrm{mod}}$. Then $\triangle\phi_i$ is the standard deviation of the distribution of factor values such as $\triangle\mathrm{POC}_i^{\mathrm{mod}}$ does not exceed the standard deviation of the experimental POC data, $\triangle\mathrm{POC}^{\mathrm{exp}}$, at

any mesocosm, at any time. This comprises a Monte Carlo non intrusive sampling base method for uncertainty quantification [Chantrasmi and Iaccarino, 2012]. The effect size of variations of ϕ_i on the variability is then

$$\varepsilon_i = \frac{(\triangle \mathrm{POC})_i^{\mathrm{mod}}}{\triangle \phi_i}. \tag{3.1}$$

This effect size expresses the maximum variability a factor can generate, $\triangle \mathrm{POC}_i^{\mathrm{mod}}$, relative to the range of factor variations, $\triangle \phi_i$, to ensure $\triangle \mathrm{POC}_i^{\mathrm{mod}}$ is the closest to $\triangle \mathrm{POC}^{\mathrm{exp}}$ at any time. More generally, ε_i relates the uncertainty of a variable X (here X =POC) and the uncertainty of the input factors ϕ_i on which it depends (that in our application quantifies how much variability in experimental observables derives from cell physiology and community structure)

$$(\triangle X)^2 = \sum_{i=1}^{N} c_i^2 \cdot (\triangle \phi_i)^2$$

where $c_i = \frac{\partial X}{\partial \phi_i}$ are called sensitivity coefficients [Ellison and Williams, 2012]. This expression is based on the assumption that changes in X in response to variations in one factor ϕ_i are independent from those due to changes in another factor ϕ_j and that all changes are small, thus cross terms and higher order derivatives are negligible. Where no reliable mathematical description of $X(\phi_i)$ exists, c_i can be evaluated directly by experiment [Ellison and Williams, 2012]. As in our case only the rate equation for POC changes is known, but not its analytical solution, and, as mentioned in the Introduction, such measurements are costly in mesocosm experiments, we obtain equivalent information through the numerical calculation of the corresponding effect sizes ε_i. In the following, the standard deviation of the factors, i.e. factors uncertainty $\triangle \phi_i$ will be given as percentage of the reference values and will be called $\triangle \Phi_i$. The actual factor range is given by: $\triangle \phi_i = \frac{\triangle \Phi_i \cdot \phi_i}{100}$. Strong heteroscedasticity, i.e. irregularities in the standard deviations of experimental POC data (see, for instance, small $\triangle \mathrm{POC}^{\mathrm{exp}}$ at day 8 in Fig. 2.2p), translates into drastically enhanced effect sizes if the model-data comparison would be done at a daily basis. For this reason we consider the temporal mean of the standard deviation per phase, i.e. prebloom, bloom, and postbloom. We inferred phases for PeECE II from [Engel et al., 2008] and for PeECE III from [Schulz et al., 2008] and [Tanaka et al., 2008]). For the first experiment, phytoplankton main bloom is estimated to occur from day 7 to day 13 and for the second experiment, from day 7 to day 11.

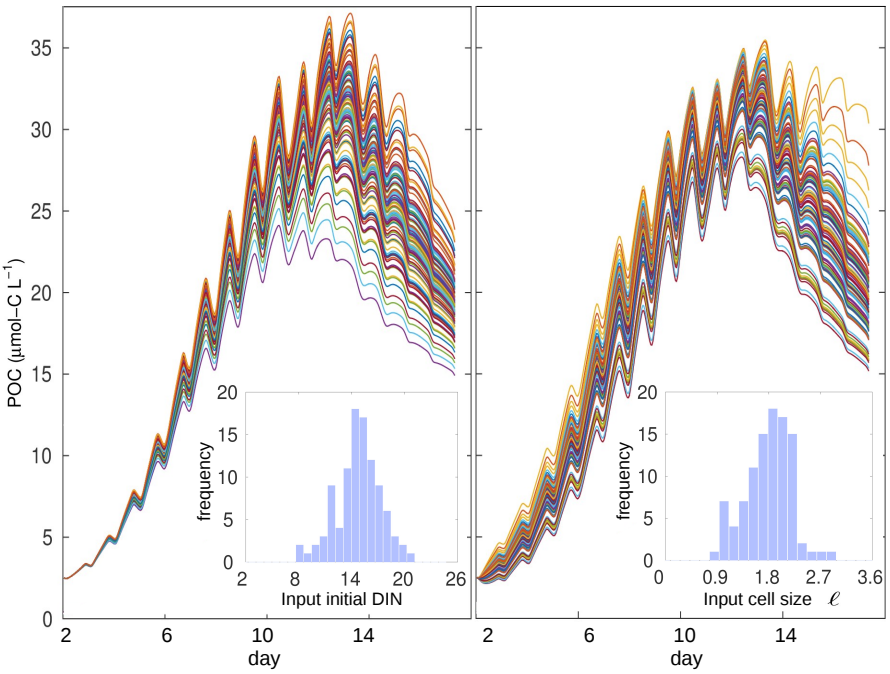

Figure 3.1. Examples of 10^2 model projections of POC for the past CO_2 treatment in PeECE III. In the left panel, model outputs with slight variations in initial nutrient concentration and in the right panel, with slight input variations in mean cell size. Histograms show input distribution with mean $\langle\phi_i\rangle$ and standard deviation $\triangle\phi_i$ given in Tables 2.1 and 3.1, respectively. To calculate system tolerances and uncertainties effect sizes, we numerically calculate 10^4 model realizations, thus the distribution of input factors is closer to normal.

To numerically calculate the ensemble of 10^4 POC trajectories that simulate experimental replicate outcomes (Fig. 3.1), we apply the Heun integration method (see Section B.1. A second order numerical method is required to obtain conservative trajectories at the chosen step length, $h = 4 \cdot 10^{-4}$ (approx. 35 seconds of experimental time) despite the presence of oscillations (see PAR forcing, Fig. A.2). The number of modeled POC time series is chosen ensuring convergence, such as a higher number of model realizations, i.e. a higher number of modeled replicates, will produce the same results.

3.2 Results

Our method allows for a factor specific variability decomposition $(\triangle\text{POC})_i^{\text{mod}}$ of the total variability in Fig. 3.2. While intensity decomposition is provided by the calcu-

lation of the effect size, also temporal decomposition is available, by grouping factors variations depending on the timing of their effect (Fig. 3.3). To identify the nature of the uncertainties (i.e. to which factor they belong to), their corresponding intensity (i.e. the effect size) and the timing of their escalation (i.e. when the variability amplification occurs) provide valuable information for experimental design and interpretation of empirical data. For example, when an experiment is designed to identify a potential effect during the bloom, uncertainties in factors triggering variability during the bloom are more relevant than the ones triggering variability during the potbloom (thus the latter need not to be subject to intensive monitoring), and among the factor uncertainties triggering variability during the bloom, we can identify which contribute the most, and consequently, we can concentrate experimental efforts in the control of these factors, when possible. If it is known that an experiment lacked accuracy in one of these factors, uncertainty propagation is then a suitable explanation for controversial conclusions extracted from statistical inference analysis, for instance, in cases when similar experiments detect an acidification effect while others fail to detect an effect (Type II error [Field et al., 2008]).

Variability during the prebloom phase can be explained mainly by variations of factors related to subsistence quota, i.e. Q^*_{subs} and α_Q in both PeECE II and III experiments (left column in Fig. 3.3). This means that variations in subsistence quota first intensify the divergence of POC trajectories, to be damped few days later by the system dynamics. These subsistence parameters only need to vary about 6% and 8% among replicates (see Table 3.1), to maximize their contribution to the $\triangle \mathrm{POC}^{\mathrm{exp}}$, thus their effect size is the highest (see Fig. 3.4). Variations in initial nutrient concentration, DIN(0), mean cell size, ℓ, and phytoplankton biomass loss coefficient, L^*, generate the modeled variability mainly during the bloom (with just about 20% differences among replicates, see Table 3.1 and second column in Fig. 3.3) showing high values of effect size (gray highlight in Fig. 3.4). Amplified variability in the postbloom phase (third column in Fig. 3.3) emerges from uncertainties in the reference temperature $\mathrm{T_{ref}}$ for the Arrhenius equation, Eq. 2.8, in sinking loss or export flux, s, and in remineralization and excretion, r^*. Effect size of $\mathrm{T_{ref}}$ is high, with just about 12% variation. To generate the high divergence during the postbloom, a strong perturbation of parameters relevant for the non phytoplanktonic biomass is needed (about 81% of the reference value for sinking and 96% for remineralization and excretion, see Table 3.1), which translates to

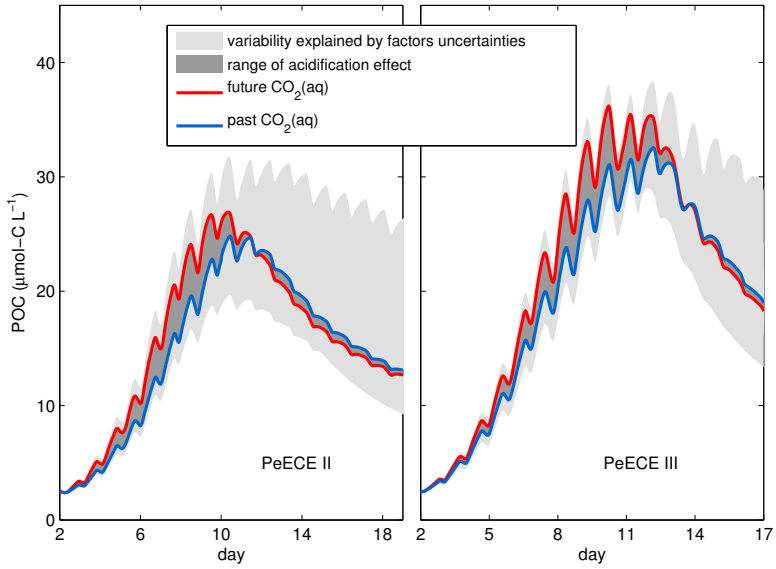

Figure 3.2. Reference simulation of POC for high CO_2 (red) and low CO_2 (blue) experimental conditions bound the range of acidification effect (dark gray) according to our model projections. Light gray is limited by the modeled POC variability, $(\triangle\mathrm{POC})^{\mathrm{mod}}$, quantified as the standard deviation of numerically simulated replicates calculated with differences in model factors simulating experimental uncertainties.

a relatively low effect size. Variability throughout all bloom phases (right column in Fig. 3.3) follows from varying carbon and nitrogen initial conditions, $\mathrm{Phy_C}$ and $\mathrm{Phy_N}$, nutrient uptake related factors, $\mathrm{V^*_{max}}$, α_V and Aff, and protein allocation for photosynthetical machinery, $\mathrm{f_p}$. About the latter, high standard deviations of the tolerance (see Table 3.1) suggests non conclusive results.

Interestingly, effect size ε_i is low for carbon acquisition $\mathrm{a_{CO2}}$ and light absorption $\mathrm{a_{PAR}}$. Perturbations of the initial detritus concentration, $\mathrm{DH_C}(0)$ and $\mathrm{DH_N}(0)$ also have no impact on the dynamics as long as they were within reasonable ranges ($\triangle\Phi_i < 100$). In fact, more than tenfold differences among replicates in such non relevant factors were necessary to achieve a perceptible $(\triangle\mathrm{POC})_i^{mod}$.

3.3 Discussion

In this study we adapted a sensitivity analysis to assess factor variations that can affect experimental data, a perspective beyond the classical description of the mean system

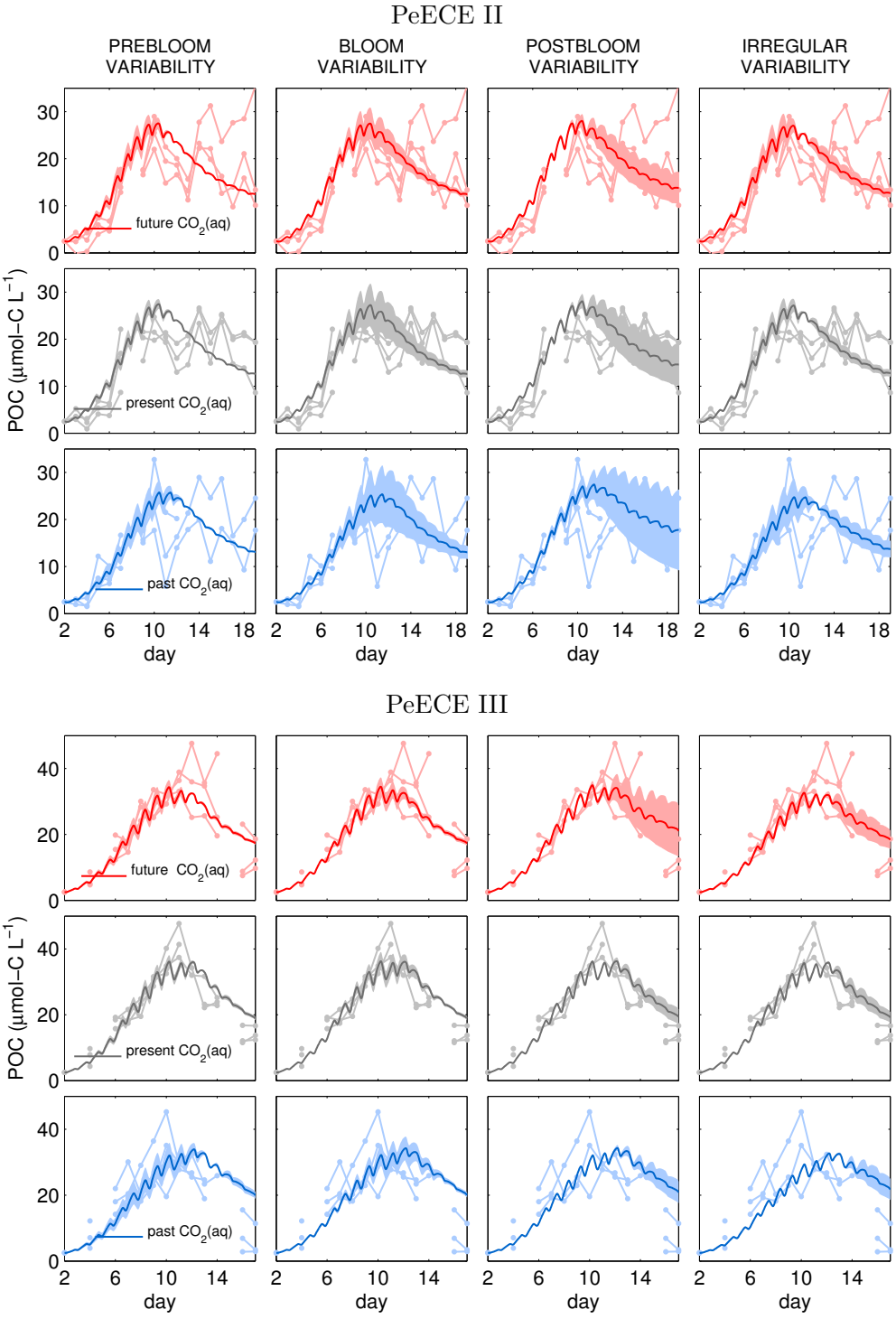

Figure 3.3. POC variability decomposition per factor, $(\triangle \mathrm{POC})_i^{mod}$. Shaded areas are bounded by the standard deviation of 10^4 modeled POC time series (see Section 3.2), around the mean trajectory of the ensemble (solid line). The timing of the amplification of the variability determines four separated kinds of behavior: factor uncertainties generating variability during the prebloom, bloom, postbloom or at irregular phase, depending on the nature and effect size of the uncertainties. For instance, bloom variability is mainly triggered by uncertainties in initial nutrient concentration, mean cell size and phytoplankton biomass losses (see Sect. 4.2).

behavior. We make use of the methodology with a low-complexity model that describes major features of phytoplankton growth dynamics and fits the mean of mesocosm experimental PeECE II and III data with high accuracy for all CO_2 treatment levels. Then we applied our approach to decompose POC variability, confirming the working hypotheses described in the introduction. In particular, we showed that small differences in initial nutrient concentration, mean cell size and phytoplankton biomass losses are sufficient to generate the experimentally observed bloom variability $(\triangle \mathrm{POC})^{\mathrm{exp}}$, Figs. 3.2, 3.4, that potentially mask acidification effects (that are higher and earlier bloom, Fig. 2.5, 2.3, with respect to less acidic environments).

3.3.1 Nutrient concentration

Differences among replicates in initial nutrient concentration substantially contribute to POC variability, a sensitivity that is, interestingly, not well expressed when varying the initial cellular carbon or nitrogen content of the algae, $\mathrm{Phy_C}(0)$ and $\mathrm{Phy_N}(0)$. The relevance of accuracy in the initial nutrient concentration in replicated mesocosms was already pointed in [Riebesell et al., 2008]. Under constant growth rate, DIN(0) determines the timing of nutrient depletion, therefore differences in initial nutrient concentrations may also translate into temporal variations in the succession of species. We not only showed that such dependence also holds in more general dynamics, but our method can also bound the variational range for differences in initial DIN concentration for experiments with low number of replicates. The standard deviation of DIN(0) in the experimental set-up for PeECE III was 50% of the mean, significantly above our tolerance threshold (see Table 3.1 for initial DIN concentration). Following [Riebesell et al., 2007], we took day 2 as initial condition, when the measured DIN was 14 ± 2 μmol-C L^{-1}. As 2 μmol-C L^{-1} is approximately the 14% of 14 μmol-C L^{-1}, replicates variability at day 2 was about a 14%. Therefore, experimental differences in initial nutrient concentration were similar to the tolerance threshold for initial DIN established to avoid high variability, $(20 \pm 6)\%$ in Table 3.1, which entails a sufficient explanation to the high divergence observed in POC measurements. For PeECE II, experimentally measured DIN concentration at day 0 was 10.7 ± 0.8 μmol-C L^{-1}, meaning a 7.5% difference among replicates, below our projected tolerance level (7.5 is out of the range $[14, 26]$). Same applies to day 2, with DIN concentration equal to 8 ± 0.5 μmol-C L^{-1}. Our approach shows that

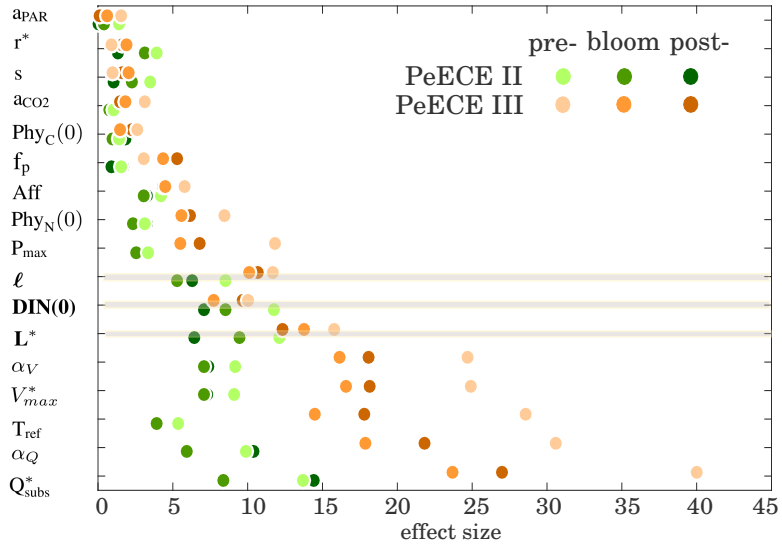

Figure 3.4. Effect size ε_i (Eq. 3.1) of variations in factors ϕ_i for different bloom phases in two OA independent mesocosm experiments. Factors whose variations trigger variability mainly during the bloom (Fig. 3.3) and potentially mask acidification effects (Fig. 3.2) are highlighted.

differences in initial nutrient concentration in PeECE II were not high enough to trigger the experimentally observed POC variability. Incidentally, there was a phosphate re-addition on day 8 of the experiment, establishing new initial nutrient concentration for the subsequent days. When the dynamics in one replicate significantly diverges from the mean dynamics of the treatment, even if the re-addition occurs at the same time and at the same concentration in all the replicates, the mesocosm with that outlier trajectory will not response as the others, and with the new nutrient condition, the divergence may be further amplified. In that case, nutrient re-addition has the same impact on the systems as variations in initial conditions of nutrient concentration. Also for PeECE II, variability in POC is about 30% higher than variability in PON, as shown in Fig. 2.2. We attribute the temporal decoupling between C and N dynamics to the break of symmetry among replicates by the nutrient re-addition due to the strong sensitivity of the system to initial nutrient concentrations and a concomitant change in subsistence N:C quota, which is a sensitive parameter, especially during the prebloom phase (Fig. 3.3 and Fig. 3.4). Increase of POC : PON ratios under nitrogen deficiency has been observed frequently during experimental studies [Antia et al., 1963, Biddanda and Benner, 1997] and has been attributed to preferential PON degradation and to intracellular decrease

of the N:C ratio [Schartau et al., 2007]. The latter process also explains the major role of subsistence quota in driving the variability (see Fig. 3.4). We hence confirm that nutrient re-addition during the course of the experiments results in a significant disturbance, as also mentioned in [Riebesell et al., 2008], although a complete analysis would require a model explicitly accounting for other nutrients, as phosphate and silicate.

3.3.2 Mean cell size as proxy for community structure

We found a limited tolerance to variations in mean cell size of the community, ℓ, which has a threshold of about 22% variation (see Table 3.1). If we take the averaged mean cell size of PeECE II, $\langle \ell \rangle = 1.6$, and III, $\langle \ell \rangle = 1.8$, from Table 2.1, we obtain $\langle \ell \rangle = 1.7$. Then the absolute standard deviation is $\triangle \ell = 22 \cdot \frac{1.7}{100} \sim 0.4$. Therefore, our methodology shows that variations within the range limited by $\langle \ell \rangle \pm \triangle \ell$, that is $[1.3, 2.1]$, are sufficient to reproduce the observed experimental POC variability during the bloom. As ℓ is in log-scale, the corresponding ESD increment is within the variational range $\langle \mathrm{ESD} \rangle \pm \triangle \mathrm{ESD}$, that is $[3.7, 8.1] \mu m$ (or $[26, 285] \mu m^3$ in volume). These values are easily reached in the course of species succession, and supports studies showing that community composition outweighs ocean acidification [Eggers et al., 2014, Kroeker et al., 2013, Kim et al., 2006].

3.3.3 Phytoplankton biomass loss

Another major contributor to POC variability during the bloom phase is phytoplankton biomass loss, L^*. With a standard deviation of about 20% (Table 3.1), uncertainties in L^* generate variability larger than the model response to OA, in particular at the end of the growth phase and the beginning of the decay phase. Unresolved details in phytoplankton loss rate include, among others, replicate differences in cell aggregation or damage by collisions, mortality by virus, parasites, morphologic malformations, or grazing by non filtered mixotrotophs or micro-zooplankton.

3.3.4 Consequences for the experimental design of mesocosm experiments

Our model projections show that a suitable target variable to detect OA effects is the slope of the bloom given by the exponential phytoplankton growth rate. We also provide

Table 3.1. Tolerance of the mesocosms to differences among replicates, given as a percentage of the reference factor $\langle\phi_i\rangle$. According to our model projections, above these thresholds $(\triangle\mathrm{POC})_i^{\mathrm{mod}}$ exceeds $(\triangle\mathrm{POC})^{\mathrm{exper}}$. In bold, main contributors to the modeled variability $(\triangle\mathrm{POC})^{\mathrm{mod}}$ during the bloom (see Sec. 3.2).

factor ϕ_i		$\triangle\Phi_i$ (%)						averaged
		PeECE II			PeECE III			tolerance
		Future	Present	Past	Future	Present	Past	(%)
$\mathrm{Phy_C}(0)$	initial phyto C biomass	68	49	46	78	60	100	67 ± 6
$\mathrm{Phy_N}(0)$	initial phyto N biomass	26	19	22	21	16	29	22 ± 4
DIN(0)	**initial DIN**	**20**	**28**	**29**	**17**	**11**	**18**	**20±6**
$\mathrm{a_{CO2}}$	carbon absorption	89	46	23	86	63	46	59 ± 23
$\mathrm{a_{PAR}}$	light absorption	>100	>100	98	>100	>100	92	> 100
$\mathrm{P_{max}}$	maximum photosyn. rate	27	18	16	22	16	28	21 ± 5
$\mathrm{Q^*_{subs}}$	subsistence quota offset	6	5	6	5	4	9	6 ± 1
α_Q	$\mathrm{Q_{subs}}$ allometry	9	7	8	7	5	10	8 ± 2
$\boldsymbol{\ell}$	**size Ln(ESD/1μm)**	**25**	**20**	**29**	**19**	**14**	**22**	**22±5**
$\mathrm{f_p}$	fraction of protein in photosyn. machinery	92	75	44	36	17	38	50 ± 25
V^*_{max}	maximum nutrient uptake	13	11	14	10	8	14	12 ± 2
Aff	nutrients affinity	39	31	42	38	36	55	40 ± 7
α_V	$\mathrm{V_{max}}$ allometry	14	11	15	10	8	14	12 ± 2
$\mathbf{L}^*$	**phytoplankton losses**	**22**	**30**	**28**	**12**	**10**	**15**	**20±8**
r^*	DIN remineralization	73	99	98	128	37	52	81 ± 31
s	DH sinking	> 100	> 100	96	> 100	61	79	96 ± 21
$\mathrm{T_{ref}}$	reference temperature	17	12	14	9	7	14	12 ± 3

thresholds to uncertainties that can be used for improving future sampling strategies with low number of replicates. These thresholds are based on our approach that for the first time quantifies how much replicates similarity can be compromised before outcomes variability outweighs potential acidification effects. Tolerances given in Table 3.1 represent theoretical thresholds for the unintended differences among replicates in experimental set-ups. Some tolerances correspond to maximal variations in observable quantities, as nutrient concentration and community composition. We show that a better control of such dissimilarities among replicates can help to keep the tolerance threshold, specially during the bloom. Strategies to reduce $(\triangle\mathrm{POC})^{\mathrm{mod}}$ should similarly apply to lower $(\triangle\mathrm{POC})^{\mathrm{exp}}$. For example, a complete characterization of phytoplankton biomass losses, which includes aggregation and grazing, is expected to limit the amplification of simulated POC variability. Uncertainties in physiological states, like differences in affinity to nutrients and subsistence quota are more difficult to measure. However, with our analysis we provide plausible explanations for negative results in the detection of potential acidification effects [Paul et al., 2015, Schulz et al., 2008, Engel et al., 2008, Kim et al., 2006, Engel et al., 2005]. In this manner, this thesis also proves the limitation of hypothesis testing tools commonly used to asses the statistical significance to effect detectability.

3.3.5 Uncertainties in non linear equations

Phytoplankton dynamics in experiments on ocean acidification is driven by processes that are non linear (i.e. effects are not proportional to their causes) and coupled (i.e. causes interact between each other) giving rise to positive or negative feed-backs. Therefore, in systems described by non linear coupled dynamical equations, as mesocosm experiments in this thesis, some perturbations of an ecological factor can be either dampened or amplified over the course of the experiment [Riebesell et al., 2008, Andersen et al., 2009, Strogatz, 2014]. Examples of filtered perturbations are shown in the left column of Fig. 3.3. Small random changes in subsistence quota trigger variability during the prebloom phase. Examples of perturbation that get amplified by the dynamics are shown in the third column of Fig. 3.3, where higher variability appear during the postbloom phase.

Our approach generates a high number of POC trajectories, each one being a potential realization of a single mesocosm experiment. Even if the distribution of input

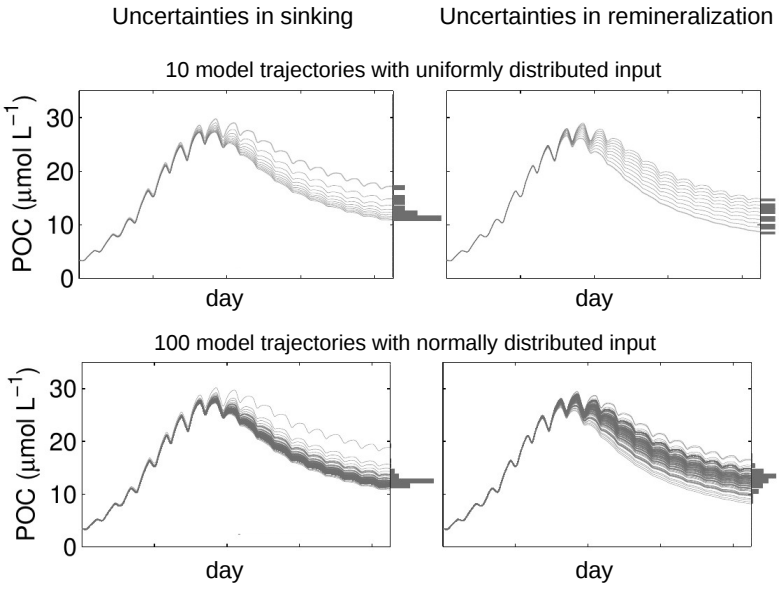

Figure 3.5. Distribution of modeled POC trajectories, each one calculated with a random value of a parameter: sinking rate, s, on the left and remineralization, r*, on the right. Right column: when applying uncertainty propagation in parameters that come linearly into the dynamics, causes are proportional to the effects. Therefore, from uniformly (top) or normally (bottom) distributed input uncertainties, we obtain uniform or normally distributed trajectories, respectively. Left column: the distribution of the outcomes at day 19 is non symmetric, independently of the input distribution, uniform (top) or normal (bottom), thus the trajectories ensemble mean and standard deviation are not representatives of the outcome distribution. The number of replicated trajectories in this figure is chosen to optimize the visibility of the distributions. For the calculation of effect sizes and confidence intervals, we simulate 10^4 replicates.

factors ϕ_i is normal, as the system is not linear, the distribution of the resulting trajectories POC^{mod} need not be normal, meaning that may not have the approximated same number of extreme events in both tails (see low row in Fig. 3.5). Uncertainties that amplify and trigger non symmetrical distributions of trajectories give rise to outliers and heavy tails, and comprise POC values that do not only differ by slight random variations that cancel out when averaging replicates results. The ensemble mean is then misleading. Solid line in Fig. 3.3, especially over the last week for future treatment in PeECE III, is higher in the third column, where results for sinking uncertainties were plotted, than for factor uncertainties triggering variability during the bloom and it does not overlap with the corresponding reference dynamics in Fig. 2.2. This shows that the trajectories distribution has not longer the reference value as an average. In fact, sinking comes non linearly into the dynamics ('s' multiplies quadratic terms of the non planktonic pools, DH), thereby its random variations generate a highly skewed POC

distribution (left column in Fig. 3.5), for normally as much as for uniformly distributed inputs. Results for variations in remineralization and excretion rates, r^*, show a linear response: uniformly distributed inputs create uniformly distributed trajectories and normally distributed inputs create normally distributed trajectories.

Therefore, under asymmetric distribution, statistical similarity among replicates is weakened, the replicates mean becomes a poor measure of the central tendency of the observed data and the standard deviation of the observations is artificially enhanced 3.6. Consequently, we observe high replicates variability that likely exceeds possible differences among treatments, which makes it difficult to draw conclusive results about the effect of the treatment. With greater trajectory dispersion a higher number of replicates with symmetrically distributed random divergent trajectories would be needed to compensate strong deviations. However, in mesocosm experiments the number of available replicates is bounded by pragmatic constrains. In such cases, the usefulness of the most common hypothesis testing tools, such as ANOVA and its variants, relies on their ability to identify an effect on a system in which their assumptions need not hold in practice. Many statistical methods assume that measurement in replicates of the same treatment only differ from the treatment mean by a quantity that follows a normal distribution, i.e. residuals must be symmetrically distributed. Such statistical tests are only asymptotically correct, thus they fail when the number of data is subcritically low, as in many mesocosm studies, even if the gaussianity of the residuals does hold. In Fig. 3.6 we show how results from 3 normally distributed replicates, in orange, still can be a poor representation of the population distribution, in green.

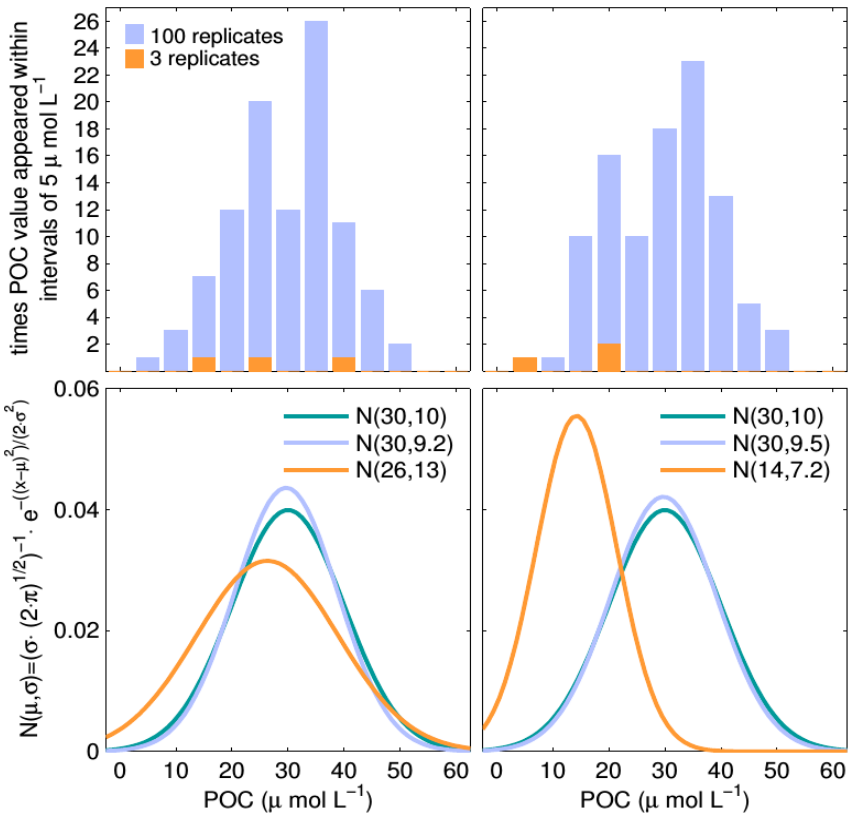

Figure 3.6. Example of POC distributions at a given day for experiments with 100 replicates (blue) and 3 replicates (orange). Solid line in green shows an example of a normalize Gaussian distribution for POC values at a given day with mean 30 μmol L^{-1} and standard deviation 10 μmol L^{-1}, usually named as N(30,10) that we take as the actual distribution of POC that day (i.e. in statistics, the green line is the distribution of the population while blue and orange lines are the distribution of 100 and 3 samples, respectively). Left: 100 random realization with values drawn from N(30,10) results in a distribution with mean 30 μmol L^{-1} and standard deviation 9.2 μmol L^{-1} (blue solid line), thus it is an accurate approximation to N(30,10). When taking only 3 random values from N(30,10), we obtain a mean equal to 26 μmol L^{-1} and standard deviation 13 μmol L^{-1} (orange solid line). Right: same procedure, just with another set of random distributed POC values. To take the mean and the standard deviation of the 3 replicates distribution is not a fair representation of the actual distribution. Besides the shift of the mean, a normal representation of the 3 times replicated sample introduces almost 30% artificially increased (left) or reduced (right) variability.

4

Propagation of time-varying uncertainties

4.1 Methods

In this thesis we reproduce how the model dynamics regulates random variations of model control factors as parameters and initial conditions to understand origins of biomass variability in mesocosm experiments. Factor variations simulate unresolved differences among experimental replicates affecting their ecological status. However, they are not necessarily constant during the course of the experiment. In fact, in Chapter 3, we assumed uncertainties in replicates are independent and normally distributed around the treatment mean, while here we also consider the uncertainties may change in time, with fluctuating between several intensities and at every frequency, an effort efficiently accomplished by the use of stochastic dynamical models.

Here we calculate the confidence intervals and effect sizes of uncertainties in model factors as in Chapter 3, although the uncertainties we introduce in the reference dynamics are time-dependent. Due to limitations that are later discussed, we need to reduce the system complexity and, instead of modeling POC dynamics, we will focus here in just phytoplankton growth and decay. As a consequence, we introduce uncertainties into the treatment dynamics described in Chapter 2.2, where the state variables are carbon and nitrogen content of phytoplankton, $\mathrm{Phy_C}$ and $\mathrm{Phy_N}$ and dissolved inorganic nitrogen, DIN. They are the y_j components of $\vec{y}$, the vector of state variables, such that

$\vec{y} = \{\text{PhyC, PhyN, DIN}\}$ with $j = 1, ..., N = 3$, whose dynamics is generically described by

$$\frac{d\vec{y}(t)}{dt} = \vec{f}(t, \vec{y}(t), \vec{\phi}) \tag{4.1}$$

with $\vec{\phi}$ the vector of model parameters as described in Chapter 3, now with ϕ_i, with $i = 1, ..., N = 14$, made of 14 process parameters. With these notation we represent the system of coupled deterministic differential equations [Boyce and DiPrima, 2012] given by Eqs. 2.6. This system is suitable for numerical solution. Common integration methods rely on the estimation of the value of the state variable at a given time step from its value at a previous time step at a distance h, such as

$$\vec{y}(t + h) = \vec{y}(t) + \vec{f}(t, \vec{y}(t), \vec{\phi}) \cdot h + \mathcal{O}[h^2] \tag{4.2}$$

(see Section B.1 for the derivation of this expression). The knowledge of $\vec{y}$ at $t = 0$, i.e. the initial conditions, allows for the calculation of subsequent steps such as the obtained time series constitutes a discretization of the solution of Eq. 4.1 at first-order of approximation. This popular procedure is known as the Euler integration method [Boyce and DiPrima, 2012]. In this thesis we use a two-stage extension providing a second-order approximation that is known as Heun method (as mentioned in Chapter 3 for the deterministic version). However, we illustrate the differences between the propagation of static and time-varying uncertainties with the Euler method to simplify the explanation,.

We consider random fluctuations of the mean behavior of each treatment described by Eq. 4.1, the reference dynamics. As in Chapter 3, ensemble averages of the replicates within a given treatment are noted in bracket. We also consider here that parameter variations ξ_ϕ are random and following a normal distribution, thus only the lowest order moments are required for the moment-generating function that completely characterize the distribution. In the simplest case, the mean of the fluctuations of a given parameter ϕ_i is chosen to be zero at any time to represent non directional departures from the mean dynamics, and fluctuations are assumed to be independent, thus the autocorrelation at different times and the cross-correlation between different parameters is zero different parameters and times

$$\begin{aligned} \langle \xi_\phi(t) \rangle &= 0 \\ \langle \xi_{\phi_i}(t) \cdot \xi_{\phi_k}(t') \rangle &= \delta_{i,k} \cdot \delta_{t,t'} \end{aligned}$$

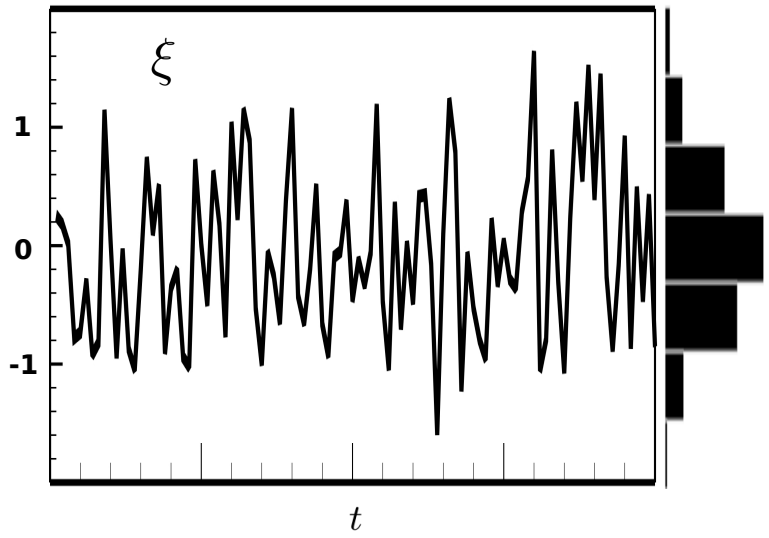

Figure 4.1: One realization of white noise.

with δ the Kroenecker's delta. Random fluctuations with such characteristics are called white noise (Fig. 4.1) since they contains fluctuations at all possible frequencies [Toral and Colet, 2014]. The amplitude of the random variable is given by the variance of the corresponding parameter such that $\phi_i = \langle\phi_i\rangle + \triangle\phi_i \cdot \xi_{\phi_i}$ represents a value of the parameter random distribution around its reference value with its confidence interval. To simulate unresolved details in ecological experiments that compromise replicates similarity, noise of this kind can be included in the dynamics in different ways.

A static representation of the uncertainties consists in selecting a value of the parameter random distribution per model realization. Then we numerically iterate the recurrence equations 4.2 to find the time series of $\mathrm{Phy_C}$ and $\mathrm{Phy_N}$ and DIN that are solution of the system equations 4.1. We repeat this calculation to generate 10^4 of such deterministic solutions, such that each realization simulates the dynamics of a virtual replicate. The noise ξ does not depend on time, only affects model initialization. That simplifies its characterization: we can considered the stochastic variable ψ as a random number. For each parameter ϕ_i, such random numbers can be simulated with values drawn from a pseudo random gaussian generator that produces u_k values with

$k = 1, ..., 10^4$ from a distribution with zero mean and unitary standard deviation

$$\begin{aligned} \langle u \rangle &= 0 \\ \langle u_k \cdot u_w \rangle &= \delta_{k,w} \end{aligned} \tag{4.3}$$

with δ the Kroenocker's delta. Then $\phi_i = \langle \phi_i \rangle + \triangle\phi_i \cdot u$ with a different value of u for each virtual replicate. Therefore, model realizations are deterministic, only the initialization is random. This approach was successfully implemented in Chapter 3 for the simulation of potential sources of variability in POC. We perform the same approach here, but with BIOACID II data set and a simplified model. This assures an optimal comparison of effect sizes and tolerance thresholds between static and time-dependent variations, both calculated based on the same data set modeled with the same reference dynamics.

As mentioned earlier in this chapter, a natural extension of the static is the simulation of unintended differences among replicates that change in time. We also simulate an ensemble of 10^4 model realizations. However, for each of them, a new selection of the parameter value is drawn from its normally distribution at every time step, not only at initialization. Variations in the parameter not only among model realizations but also in time brings stochasticity to the model and implies parameters become time-dependent. However, they remain parameters, not state variables, since we do not attempt to describe their dynamics apart from their random fluctuations. We just assume that in every given virtual replicate, the value of the parameter changes randomly in time. Noise is introduced in the dynamics by substituting ϕ_i by $\phi_i(t) = \langle \phi_i \rangle + \triangle\phi_i \cdot \xi_{\phi_i}(t)$ in Eq. 4.1.

$$\frac{d\vec{y}(t)}{dt} = \vec{f}(t, \vec{y}(t), \langle \phi_i \rangle + \triangle\phi_i \cdot \xi_{\phi_i}(t)). \tag{4.4}$$

Then, depending on if this system of coupled differential equations is solved with stochastic numerical methods or it is solved as if it would be deterministic (i.e. without any modification of Eq. 4.2), the uncertainty propagation is called intrusive or not intrusive (to the dynamics), respectively.

4.1.1 Intrusive method

In an intrusive method, each model realization is numerically obtained by solving Eq. 4.4 after separating the deterministic and the stochastic parts

$$\frac{d\vec{y}(t)}{dt} = \vec{f}(t,\vec{y}(t),\langle\vec{\phi}\rangle + \triangle\vec{\phi}\cdot\xi_\phi(t)) = \vec{q}(t,\vec{y}(t),\langle\vec{\phi}\rangle) + \vec{g}(t,\vec{y}(t),\triangle\vec{\phi})\cdot\xi_\phi(t). \tag{4.5}$$

Stochastic differential equations in which such separation is possible are known as the Langevin equations. Vectorial functions with components q_j and g_j are known as drift (or the deterministic term) and diffusion (or the uncertainties term), respectively [Toral and Colet, 2014]. An example of how the disentanglement works is provided in Appendix B.2. Stochastic equations where the separation of $\vec{f}(t,\vec{y}(t),\vec{\phi})$ into $\vec{q}(t,\vec{y}(t),\langle\vec{\phi}\rangle)$ and $\vec{g}(t,\vec{y}(t),\triangle\vec{\phi})$ is not possible cannot be represented as Langevin equations. This is the case of many parameters in our system, for instance, the component of the vector parameter corresponding to size, $\phi_i = \ell$, does not reproduce Eq. 4.5 when substituting $\vec{\phi}$ for an identical vector but with the size component $\ell = \langle\ell\rangle + \triangle\ell\cdot\xi_\ell$. Then advance methods, including the discretization of the solution into the randomness dimension, are required [Ghanem and Spanos, 1991, Constantine et al., 2010, Chantrasmi and Iaccarino, 2012] but they are out of the scope of this thesis, thus we limit our analysis to the parameters that allows the linear sepatation given in Eq. 4.5. In this work we use a multidimensional stochastic Heun algorithm [Toral and Colet, 2014] to numerically solve Langevin equations. However, to simplify, we show here a first-order approximation, known as Mishtein algorithm, that is the stochastic version of Eq. 4.2. For an optimal notation, we describe the solution for one state variable

$$\begin{aligned} y_j(t+h) &= y_j(t) + q_j(t,\vec{y}(t),\vec{\phi})\cdot h + g_j(t,\vec{y}(t),\vec{\phi})\cdot\sqrt{h}\cdot u_f + \\ &+ \frac{h}{2}\cdot u_k\cdot u_w\cdot\Big(\sum_{N=1}^{N=3} g_N(t,\vec{y}(t),\vec{\phi})\cdot\frac{\partial g_j(t,\vec{y}(t),\vec{\phi})}{\partial y_N}\Big|_{t,\vec{y}(t),\vec{\phi}}\Big) + \mathcal{O}[h^2] \end{aligned} \tag{4.6}$$

where u are again random numbers with moments defined in 4.3. See Appendix B for the derivation of this expression. Special attention must been paid in the transition from the stochastic variable ψ to the random number. A deterministic model is obtained for null diffusion terms, $\vec{g} = 0$, thus Eq. 4.2 is recovered. When the diffusion term is a scalar, last row in Eq. 4.6 vanished and the noise is additive (and the solution resemble Eq. 4.8 for the non intrusive method). Otherwise the noise is multiplicative, the derivatives of the drift term with respect to the state variables are non zero, meaning we account for

the coupling between noise and the dynamics of the state variables.

4.1.2 Non intrusive method

In an non intrusive method, each model realization is similar to Eq. 4.6, only different in the way it is solved due to a different noise implementation

$$\frac{d\vec{y}(t)}{dt} = \vec{f}(t, \vec{y}(t), \langle\phi_i\rangle + \triangle\phi_i \cdot \xi_{\phi_i}) = \vec{f}(t, \vec{y}(t), \langle\phi_i\rangle + \triangle\phi_i \cdot u) \tag{4.7}$$

that is, at each time step, noise is directly simulated as a pseudo random variable u characterized by Eqs. 4.3 instead of thus the recurrence equation for the solution yields

$$\vec{y}(t+h) = \vec{y}(t) + \vec{f}(t, \vec{y}(t), \langle\phi_i\rangle + \triangle\phi_i \cdot u) \cdot h + \mathcal{O}[h^2]. \tag{4.8}$$

Therefore, there is not coupling between noise and the dynamics of the state variables.

We apply static and time-varying uncertainties to reveal major contributors to the variability in BIOACID II indoor data. We identify those parameters whose uncertainties generate the maximum variability $\triangle\mathrm{Phy_C}$ with the minimum variational range $\triangle\phi_i$ (variational ranges listed in Table 4.1). To that aim, we calculate the effect size of the uncertainties on the variability with Eq.3.1 as in Chapter 3.

4.2 Results

Our model-based data analysis explores which uncertainties in parameters potentially raise sufficient variability in the distribution of phytoplankton biomass between replicates, $\triangle\mathrm{Phy}^{mod}_{\mathrm{C,i}}$, to overcome treatment effects. We perform the analysis propagating static uncertainties (deterministic approach) and time-varying uncertainties (stochastic approaches). The comparison among methods are limited by the intrusive method, that is suitable to describe only uncertainties that come linearly into the dynamics (see Section B.2). Therefore, we only apply uncertainty propagation in subsistence quota, $\mathrm{Q}^*_{\mathrm{subs}}$, maximum primary production rate, $\mathrm{P_{max}}$, fraction of protein allocation for photosynthesis, $\mathrm{f_p}$ and phytoplankton biomass losses, L^*.

Effect sizes for the three different approaches are presented in Fig. 4.3, showing that uncertainties in subsistence quota and maximum uptake rate are relevant sources of variability. About a timing-based decomposition, Fig. 4.2 shows that variations in Q^*_{subs} and P_{max} mainly contribute to variability during the growing phase, uncertainty in f_p triggers irregular variability and differences in L^* promote divergences during the bloom. As temperature and acidification mainly affects the bloom (see Fig. 2.5), we confirm results given in Chapter 3 revealing that uncertainties in phytoplankton biomass losses potentially mask treatment effects. About an intensity-based decomposition, we show significant differences in confidence intervals depending on the approach (see standard deviations of the histograms of the inputs distributions in Fig. 4.2 and Table 4.1). Static uncertainties show values close to the tolerances previously found with static uncertainties in PeECE experiments (Chapter 3). However, with time-varying uncertainties, confidence intervals are higher for both, the intrusive and the non intrusive method.

4.3 Discussion

4.3.1 Comparison between methods

As mentioned before, our calculations for the tolerance of mesocosm experiments to unresolved ecological details that compromise replicates similarity significantly change from simulations accounting for deterministic or stochastic uncertainties. Static uncertainties present lower confidence intervals than for the time-varying uncertainty models, being the non intrusive method the one depicting the highest tolerances (see Table 4.1 and Fig. 4.2).
When taking the ensemble average of Eq. 4.6 for the 10^4 model trajectories

$$\begin{aligned}\langle y_j(t+h)\rangle &= \langle y_j(t)\rangle + q_j(t,\vec{y}(t),\vec{\phi})\cdot h + g_j(t,\vec{y}(t),\vec{\phi})\cdot\sqrt{h}\cdot\langle u_f\rangle + \\ &+ \frac{h}{2}\cdot\langle u_k\cdot u_w\rangle\cdot\Big(\sum_{N=1}^{N=3} g_N(t,\vec{y}(t),\vec{\phi})\cdot\frac{\partial g_j(t,\vec{y}(t),\vec{\phi})}{\partial y_N}\Big|_{t,\vec{y}(t),\vec{\phi}}\Big) + \mathcal{O}[h^2]\end{aligned}$$

we recover the solution for the reference run, Eq. 4.2, i.e. the noise-free limit. Therefore, intrusive methods are conservative as long as the number of replicates is high enough to ensure Eqs. 4.3 stand. For the non intrusive method, Eq. 4.8, when function $\vec{f}(t,\vec{y}(t),\vec{\phi}_i)$

depends linearly on the parameter and its noise, i.e. $\phi_i = \langle\phi_i\rangle + \triangle\phi_i \cdot \xi_{\phi_i}$ (that for non intrusive method is just $\phi_i = \langle\phi_i\rangle + \triangle\phi_i \cdot u$), a separation of deterministic and stochastic parts yields

$$\vec{y}(t+h) = \vec{y}(t) + \vec{q}(t, \vec{y}(t), \langle\phi_i\rangle) + \vec{g}\,'(\triangle\phi_i \cdot u) \cdot h + \mathcal{O}[h^2]. \tag{4.9}$$

Note that, while the drift term is the same than for the intrusive method, the stochastic part is different (see drift and diffusion terms defined in Eq. 4.5). In particular, this expression does not comprise the derivatives accounting for the coupling among state variables and noise, a feature expressed with rigor in Eq. 4.6 for the intrusive method. This underestimation of the noise impacts on the dynamics smooths the chance for divergent trajectories. Therefore, same standard deviations of the model outcomes are achieved as for the intrusive model but with much higher variational range for the parameters (see Fig. 4.2 and Table 4.1. This explains why confidence intervals $\triangle\phi_i$ calculated with the non intrusive method are higher than for the intrusive approach, resulting in an extremely low effect size, Fig. 4.3. Moreover, the ensemble average of the solution is

$$\langle\vec{y}(t+h)\rangle = \langle\vec{y}(t)\rangle + \vec{q}(t, \vec{y}(t), \langle\phi_i\rangle) + \langle\vec{g}\,'(\triangle\phi_i \cdot u)\rangle \cdot h \tag{4.10}$$

where we cannot assure that the last term is zero in average in order to recover Eq. 4.2, thus non intrusive methods not necessarily preserve the dynamics of the free-noise limit. This is particularly relevant for large parameter confidence intervals $\triangle\phi_i$ and low number of virtual replicates. Same applies to the deterministic approach for static uncertainties since nothing ensures that the ensemble average of the 10^4 overlaps the reference dynamics. When the parameter is directly proportional to a state variable that significantly changes in time, an uncertainty propagation method different from 4.6 generates artificial departures from the reference run that do not cancel out when averaging, thus the standard deviation of the ensemble model outcomes is larger. This may explain why variational range of P_{max} (just linear in primary production, Eq.2.7) is higher for the deterministic and non intrusive approaches.

4.3.2 Consequences for modeling

Popular methods to numerically solve systems of differential equations rely in discretization of the dynamics to obtain recurrence expressions that are more or less sophisticated

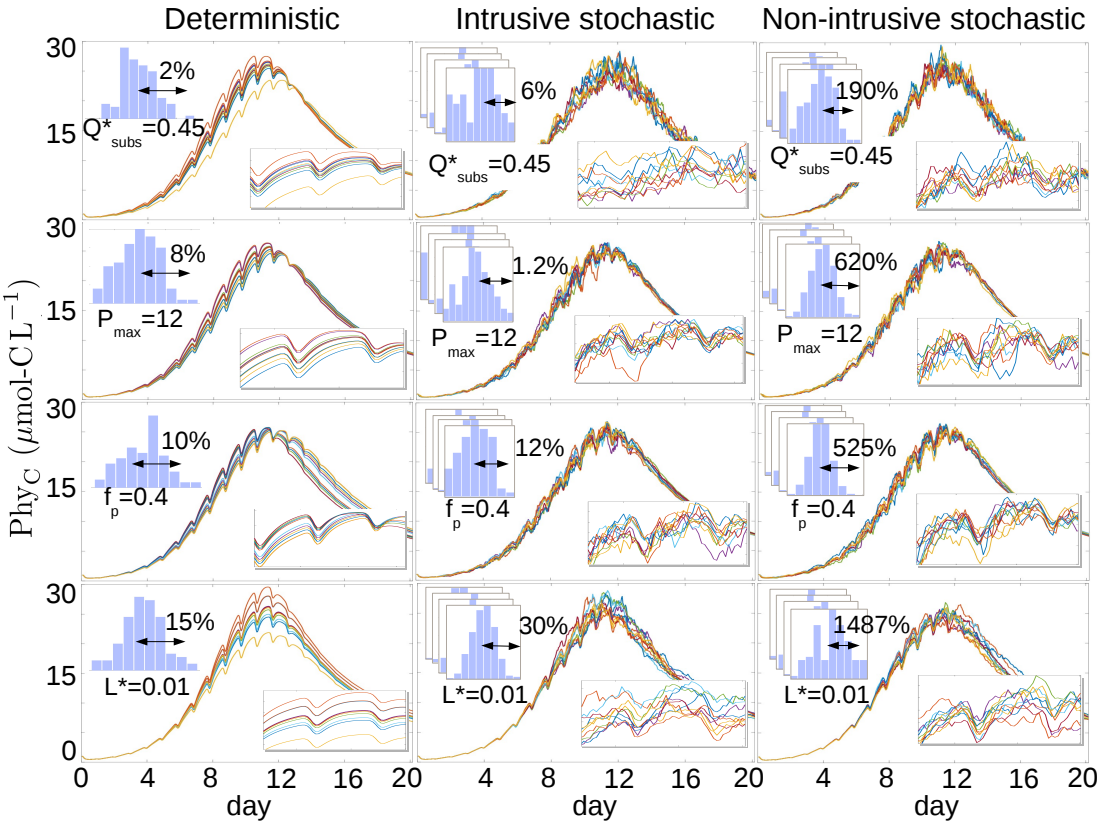

Figure 4.2. Ensemble of 10 model trajectories of phytoplankton carbon for each parameter following the three different uncertainty propagation methods we analyzed. Histograms show inputs distribution, with means is given in Table 2.2 and the standard deviations in Table 4.1. For the deterministic approach, only one distribution setting the initial parameters values is required while one different distribution is taken every time step in the stochastic approaches. Days 10 and 11 are shown in detail as inset.

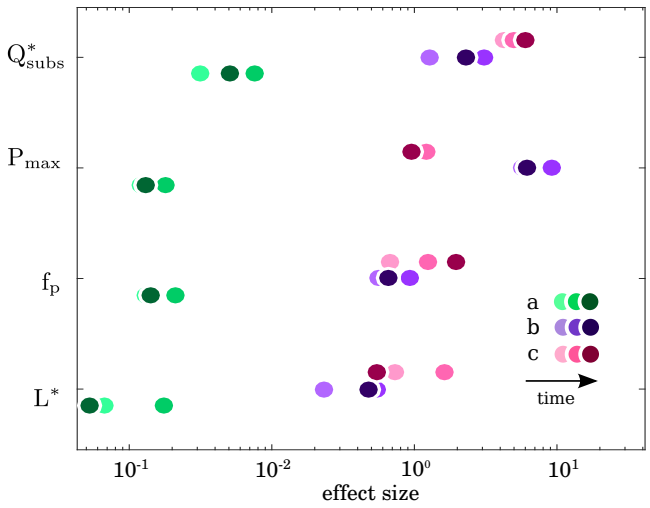

Figure 4.3. Effect size ε_i of parameters uncertainties on the phytoplankton variability. a) static uncertainties (deterministic approach) and time-varying uncertainties with: b) stochastic intrusive approach and c) stochastic non intrusive approach. As in Fig. 3.4, the effect size a parameter is calculated for the prebloom, the bloom and the postbloom, with time increasing with color darkness.

versions of Eq. 4.2. They are based on a projection of the value of the solution at the next time step estimated from the rate of change of the variable and its value at a previous step. An effective use of these methods requires the solution to be smooth and differentiable, thus sharp changes in the dynamics leads to departures from the right trajectory when a proper modification of the numerical method is dismissed. If a generic function $f(t, \vec{y}, \vec{\phi})$ in Eq. 4.1 contains any kind of noise (i.e. sharp, quick changes of its values at h scales) and that fluctuation gives rise, for instance, to a sudden high value of f, when introducing that value in an equation as Eq. 4.2 or similar, the projected new step will be artificially higher. A new fluctuation in f in the opposite direction not necessarily compensate the deviation. Such spontaneous correction depend on non linearities in the model equations, noise distribution and how the noise came into the mathematical expression of f. Situations like that are common in ecosystem models, where forcing data (temperature, wind, PAR,...) are introduced as parameters ϕ in differential equations like 4.1. Random fluctuations in such observational data may produce misleading results if we attempt to solve the system with a deterministic or non intrusive integration method.

Moreover, as non intrusive methods dismiss relevant terms of the solution (compare

Eq. 4.6 and Eq. 4.9), they may not properly account for the whole complexity of the system and, as we showed, the effects of the noise are smoothed. Sensitivity analysis based on non intrusive methods may entail artificially enlarged confidence intervals when exploring variational ranges of parameters.

Table 4.1. The standard deviation of the possible values for each factor, $\triangle\phi_i$, is given as a percentage of the reference factor value and defines the confidence interval of the tolerance of the system to variations in each factor.

		average tolerance (in % of $\langle\phi\rangle_i$)		
		static uncertainty (deterministic)	time-varying uncertainty (stochastic)	
factor ϕ_i			intrusive	non intrusive
Q^*_{subs}	subsistence quota	2	6	190
P_{max}	max. photosyn. rate	8	1.2	620
f_p	protein allocation	10	12	525
L^*	phyto. biomass losses	15	30	1487

4.3.3 Consequences for the experimental design of mesocosm experiments

Heuristic constrains to the number of replicates makes difficult to explore sensitivities of mesocosm experiments to input fluctuations. With our model we provide an estimation of the tolerance of the mesocosm to unresolved details in different ecological factors. Above such thresholds, uncertainties trigger variability that overweights acidification and warming effects. For instance, our variability decomposition for the stochastic intrusive method suggests that differences among same treatment replicates in phytoplankton biomass losses above 30% of the mean value in the treatment are sufficient to hinder the detection of a treatment response that can be attributed to acidification and/or warming. L^* mainly parametrizes grazing pressure. In [Horn et al., 2015] relevant information about mesozooplankton dynamics in the experiment is provided, however, only replicate differences for cilliate biomass are shown. They are represented by the standard deviation of the biomass values within replicates distribution, that during the bloom was above 30% of the treatment. Incidentally, other parameters representing

features of cell physiology and community composition as subsistence quota, fraction of protein allocation for photosynthesis are difficult to measure and no experimental data are available. From our intrusive stochastic method we estimated that replicates dissimilarities above 1.2% of the mean of the treatment in grazing is the main cause of phytoplankton biomass removal are sufficient to reproduce the variability observed in phytoplankton carbon. If we take growth rates given in [Paul et al., 2015] as a proxy of P_{max}, we see that the variations in experimental data exceeded the limits estimated by our confidence interval. Therefore, our analysis suggests plausible explanations for negative results in the detection of multi-stressors effects and provides useful thresholds for future sampling strategies.

5

Conclusions

Unobservable differences in the biological status of replicate mesoscoms, that are non-necessarily linked to the treatment effect and may not be homogeneously distributed, may create divergence in the outcomes. As mesocosm preparation and monitoring are costly and time-consuming, such experiments are functionally limited to very few replicates per treatment. Under such circumstances, mechanistic models are a plausible alternative to post-processing tools. Our model projections for biomass growth and decay in mesocosm experiments on OA indicate that phytoplankton responses are mainly expected to occur during the bloom phase, showing a higher and earlier bloom under acidification conditions, even if no effect was detected by statistical inference analysis of the same data [Schulz et al., 2008, Engel et al., 2008]. Our results also suggest that this effect is less relevant in mesocosms exposed not only to high CO_2 concentrations but also high temperatures. We thereby reveal potential synergistic effects between acidification and warming where hypothesis testing tools fail to detect a significant statistical response [Paul et al., 2015].

Moreover, we found that amplified biomass variability during the bloom can be explained by variations in initial DIN concentration, mean cell size and the phytoplankton loss rate, which are related to cell physiology and community composition. According to our model projections, differences in such factors between replicates should be confined, otherwise acidification responses are likely to be masked by outcome variability. We provide the confidence intervals for the uncertainties, which serve as an estimation of the tolerance thresholds. Below these thresholds, accidental underlying heterogeneity will

not escalate into high variability. Our analysis of experimental data from mesocosms with low numbers of replicates per treatment shows that when replicate dissimilarities in initial nutrient concentration, mean cell size or phytoplankton biomass losses have standard deviations greater than $\sim 20\%$ of the mean value they take in the treatment, outcome variability hinders the detection of a potential acidification effect. These results may help in the development of prevention interventions to avoid uncertainties escalation and enhance the detection of potential responses.

Interestingly, when applying time-varying uncertainty quantification, the confidence interval of parameters was enlarged in comparison to the case of static uncertainties. This means that mesocosms are more tolerant to time-dependent underlaying heterogeneity between replicates. This finding comprises consequences not only for experimental design but also for model parametrization based. Sensitivity analysis based on static uncertainty propagation methods may underestimate confidence intervals of parameters while solutions of model equations comprising random values (for instance for wind, PAR, salinity concentration,...) may generate overestimated confidence intervals of parameters when calculated by non intrusive numerical methods.

Our modeling of the propagation of static uncertainties with a deterministic equations revealed cell size to be a major contributor to the phytoplankton biomass variability, which promotes the use of an adaptive trait-based dynamics models to resolve ecophysiologial trait shifts in non-stationary scenarios [Wirtz and Eckhardt, 1996, Wirtz, 2013]. This would provide a dynamical equation for the rate of change of size, thereby making a study of the propagation of time-varying uncertainties in cell size are straight forward to implement. Extensions comprising covariance matrices showing the interaction of variations in two factors simultaneously are also suitable in our static and time-varying approaches to uncertainty propagation.

In addition, we show that uncertainty propagation can also complement sensitivity analysis to test robustness of both experiments and model runs to static and time-varying uncertainties. Intrusive methods provide a more rigorous estimation of parameter confidence intervals for model calibration. This improvement is expected to be general for a large group of models with stochastic components. Uncertainty propagation using different model formulations (not shown here) led to quantitatively different confidence intervals, while qualitative results remain unchanged.

Finally, this study established a foundation for further model-based analysis of uncertainty propagation that can be generalized to any kind of experiments in biogeoscience. We argue that a more explicit description of uncertainty quantification is pivotal in our interpretation and generalization of experimental results.

A

Appendix

A.1 Residuals of the model-data fit

We calculate the cumulative residuals with respect to the mean of experimental replicates per treatment, time and mesocosm. For experimental data

$$\mathrm{E} = \sum_{\mathrm{treat,rep,day}} |\mathrm{Y}^{\mathrm{exp}}_{\mathrm{treat,rep,day}} - \langle \mathrm{Y}^{\mathrm{exp}}_{\mathrm{treat,day}} \rangle| / \eta$$

and for model results

$$\mathrm{M} = \sum_{\mathrm{treat,rep,day}} |\mathrm{Y}^{\mathrm{mod}}_{\mathrm{treat,rep,day}} - \langle \mathrm{Y}^{\mathrm{exp}}_{\mathrm{treat,day}} \rangle| / \eta$$

being η the number of mesocosms (9 for PeECE III experiment and 11 for BIOACID II experiment since we dismiss a replicate for the low temperature and CO_2 concentration due to a lamp malfunctioning). High residuals entail high deviation from the trend. In the case of E, that means deviation from the mean of the treatment (typically use in statistical inference tools), and in the case of M, deviation from the model reference run. When both E and M values are comparable, we can infer that the quality of both representations is similar (see Tables A.1). Thus, conclusions inferred from both approaches are based on equally valid assumptions.

Y	E	M	units
POC	35.1	37.4	μmol-C L^{-1}
PON	6.0	9.1	μmol-N L^{-1}
DIN	6.7	9.2	μmol-N L^{-1}

Y	E	M	units
Phy_C	42.4	44.4	μmol-C L^{-1}
Phy_N	15.5	15.9	μmol-N L^{-1}
DIN	4.5	6.8	μmol-N L^{-1}

Figure A.1. Cumulative residuals for model-data fit with PeECE III (left table) and BIOACID II (right table) experiments.

A.2 Forcings

Measured aquatic CO_2, temperature and photosynthetic active radiation, PAR, are used as model inputs (see Fig. A.2). For the two PeECE experiments the photon flux density was measured by the Geophysical Institute of the University of Bergen. To calculate the surface radiation inside the mesocosms, PAR_0, we follow [Schulz et al., 2008] and consider that 80% of incident PAR passed through the gas tight tents of which up to 15% penetrated into c.a. 2.5 m depth, the center of the mixed surface layer in PeECE III. Daily carbon dioxide data were interpolated and the PAR signal was filtered by singular spectrum analysis to avoid sudden changes that could be detrimental for the performance of the numerical calculation since the Heun method requires differentiable functions. The photon flux density for the BIOACID II experiment was provided by lamps with a light:dark cycle of 11h50min:12h10min and maximum intensity of $252\mu molm^{-2}s^{-1}$. Temperatures were set 9 Celsius for the cold and 15 Celsius for the warm treatment [Paul et al., 2015], see Fig. A.2. Daily carbon dioxide data were interpolated to avoid sudden changes that could be detrimental for the performance of the numerical calculation since Heun method requires differentiable functions and the PAR data showed some abrupt changes (see for instance Fig. 2 in [Schulz et al., 2008]).

A.3 Data adjustments

Model equations for PeECE II and III attribute phytoplankton, detritus, and herbivorous heterotrophs to particulate organic matter. Measurements of POC also include some

fractions of large bacterioplankton, carnivorous zooplankton, as well as extracellular gel particles like transparent exopolymer particles. These additional organic contributions to POC measurements are not explicitly resolved in our model. For comparisons between simulation results and observations we therefore have to adjust the POC data. First, we remove refractory material by subtracting first day measurements as in [Riebesell et al., 2007]. Then we used data of transparent exopolymer particles (TEP) of [Egge et al., 2009] for adjusting PeECE III POC measurements. For PeECE II, POC = POC'- POC", where POC are represented by dots in Figs. 2.2, POC' are raw data from PANGAEA and POC" are the difference between particle abundance, PA, of the Coulter Counter measurements and the Flow Cytometry data in [Engel et al., 2008]:

$$\text{POC"} = \beta \cdot (\text{PA}_{\text{ Coulter Counter}} - \text{PA}_{\text{ Flow Cytometry}}).$$

The scaling parameter β=0.000065 μmol-C^{-1} L was tuned to provide reductions between 40 and 50% from total POC, in agreement with adjustments of PeECE III.

For the BIOACID II indoor experiment accurate data for phytoplankton carbon content allows as to focus in the description of phytoplankton instead of POC. However, experimental data for phytoplankton nitrogen content, Phy_N, are not available, we adjusted Chl-a experimental data by the nitrogen to Chl-a quota (for phytoplankton) given in [Wirtz and Pahlow, 2010].

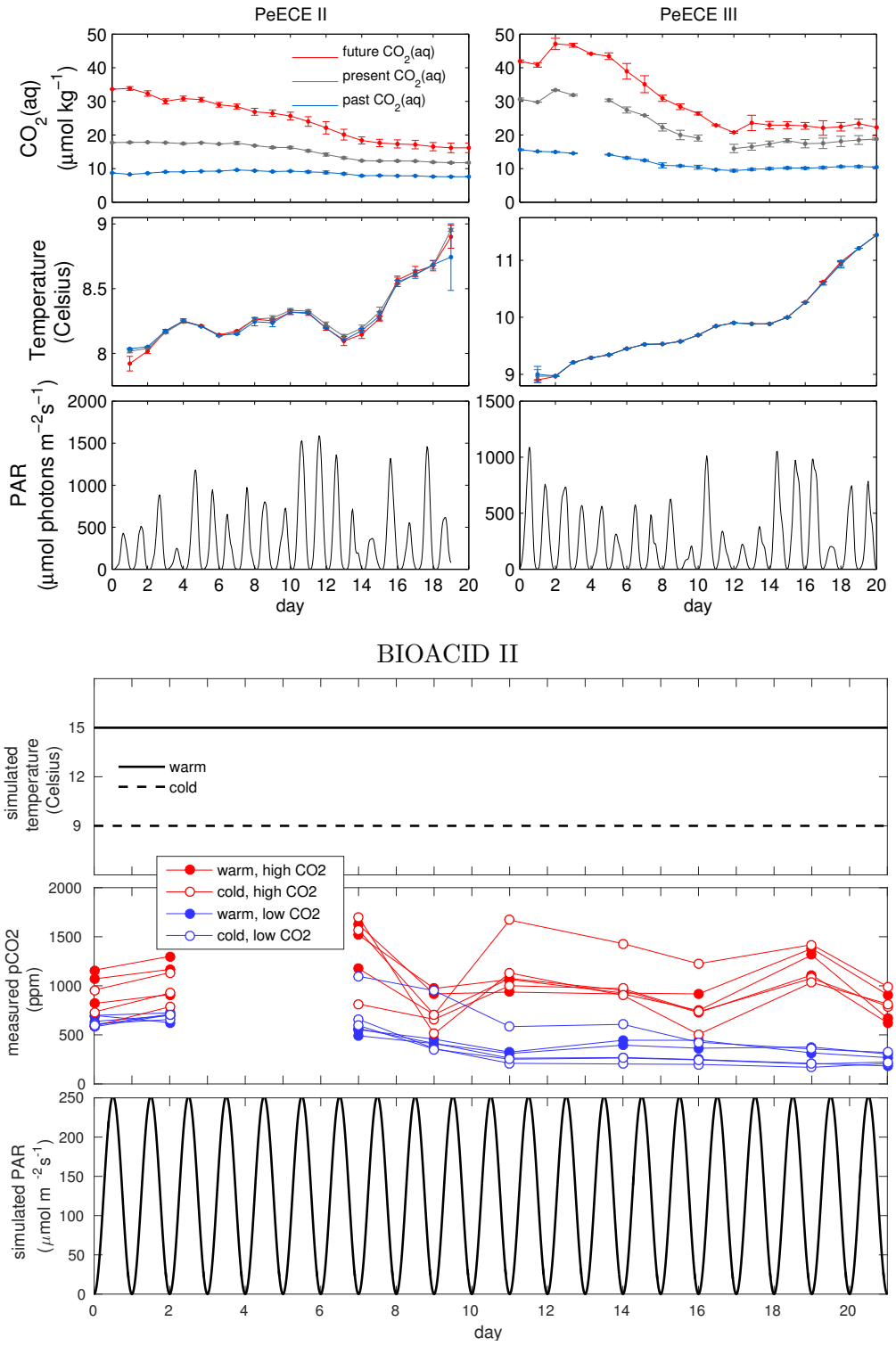

Figure A.2. Environmental data from PeECE II, III and BIOACID II are taken as model inputs. Error bars denote the standard deviation of the same treatment replicates.

B

Appendix

B.1 Derivation of numerical of solutions

To numerically solve Eqs. 4.1 and 4.5 we first integrate and obtain the analytical exact solution for one state variable (for simplicity in the notation we omit the subscript i and the explicit dependence on the parameters $\vec{\phi}$)

$$\begin{aligned} y(t+h) &= y(t) + \int_t^{t+h} q(s, \vec{y}(s))ds \qquad \text{(DET)} \\ &\quad + \int_t^{t+h} g(s, y(s)) \cdot \xi(s) \cdot ds \qquad \text{(STO)} \end{aligned} \tag{B.1}$$

where second row applies only for the stochastic model. A Taylor expansion of the drift and diffusion terms around time t yields

$$\begin{aligned} q(s, y(s, \vec{y}(s))) &= q(t, y(t, \vec{y}(t))) \\ &\quad + \sum_{m \neq i} \frac{\partial q(t, \vec{y}(t))}{\partial y_m(t)}\Big|_{t,\vec{y}(t)} \cdot (y(s) - y(t)) + h[\mathcal{O}^2] \qquad \text{(DET)} \end{aligned} \tag{B.2}$$

$$\begin{aligned} g(s, y(s, \vec{y}(s))) &= g(t, y(t, \vec{y}(t))) \\ &\quad + \sum_{m \neq i} \frac{\partial g(t, \vec{y}(t))}{\partial y_m(t)}\Big|_{t,\vec{y}(t)} \cdot (y(s) - y(t)) + \mathcal{O}[h^2] \qquad \text{(STO)} \end{aligned} \tag{B.3}$$

where only orders below $h[\mathcal{O}^2]$ are non neglected. Substituting in Eq.B.1 and keeping until order h

$$\begin{aligned} y(t+h) &= y(t) + \int_t^{t+h} q(t,\vec{y}(t)) \cdot ds \\ &+ \sum_{m\neq i} \int_t^{t+h} \frac{\partial q(t,\vec{y}(t))}{\partial y_m(t)}\Big|_{t,\vec{y}(t)} \cdot (y(s)-y(t)) \cdot ds \qquad \text{(DET)} \\ &+ \int_t^{t+h} g(t,\vec{y}(t)) \cdot \xi(s) \cdot ds \\ &+ \sum_{m\neq i} \int_t^{t+h} \frac{\partial g(t,\vec{y}(t))}{\partial y_m(t)}\Big|_{t,\vec{y}(t)} \cdot (y(s)-y(t)) \cdot \xi(s) \cdot ds \quad \text{(STO)} \\ &+ \mathcal{O}[h^2]. \end{aligned}$$

Functions non-depending on s can be move out of the integration in ds, leaving

$$\begin{aligned} y(t+h) &= y(t) + q(t,\vec{y}(t)) \cdot \int_t^{t+h} ds \\ &+ \sum_{m\neq i} \frac{\partial q(t,\vec{y}(t))}{\partial y_m(t)}\Big|_{t,\vec{y}(t)} \cdot \int_t^{t+h} (y(s)-y(t)) \cdot ds \qquad \text{(DET)} \\ &+ g(t,y(t)) \cdot \int_t^{t+h} \xi(s) \cdot ds \\ &+ \sum_{m\neq i} \frac{\partial g(t,\vec{y}(t))}{\partial y_m(t)}\Big|_{t,\vec{y}(t)} \cdot \int_t^{t+h} (y(s)-y(t)) \cdot \xi(s) \cdot ds \quad \text{(STO)} \\ &+ \mathcal{O}[h^2]. \end{aligned}$$

As $\int_t^{t+h} ds = h$ and we keep until order h, from the first row we recover Euler algorithm, the one component version of Eq. 4.2. For the stochastic part we need the definition of the Wiener process $\int_t^{t+h} \xi(s) \cdot ds = \sqrt{h} \cdot u(t)$ (Stratonovich definition) with u pseudo random normal distributed variable as described before (Eqs. 4.3). We also require another Taylor expansion, this time the state variable around t until order h

$$y(s) = y(t) + q(t,\vec{y}(t)) \cdot h + g(t,\vec{y}(t)) \cdot \int_t^s \xi(v) \cdot dv + \mathcal{O}[h^2]$$

thus last term in Eq. B.4 yields

$$g(t,\vec{(t)}) \cdot \int_t^{t+h} \int_t^s \xi(s) \cdot \xi(v) \cdot dv \cdot ds = \frac{h}{2} \cdot u_k \cdot u_w \cdot g(t,\vec{y}(t)). \tag{B.4}$$

Substituting this in Eq. B.4 we obtain the Milshtein algorithm, the one component version of Eq. 4.6. Numerical error of the stochastic part at every time step is in the

order of $h^{3/2}$. It can be shown [Toral and Colet, 2014] that the error in the moments calculation, in our case, the mean over realizations of the virtual replicates ensemble, $\langle y_j \rangle$, and the corresponding variance, $(\triangle y_j)^2$, is proportional to h^2 and, after the total time steps, the cumulative error in the moments is of the order of h.

B.2 Identification of drift and diffusion terms

We take as example the simulation of unresolved details in phytoplankton biomass losses, thus we focus in the propagation of uncertainties in the component $\phi_i = \mathrm{L}^*$ of the parameter vector $\vec{\phi}$, with $\mathrm{L}^* = \langle \mathrm{L}^* \rangle + \triangle \mathrm{L}^* \cdot \xi_\mathrm{L}$. As explained before, Eqs. 2.6 can be represented in vector notation with $\vec{y} = \{\mathrm{PhyC}, \mathrm{PhyN}, \mathrm{DIN}\}$ and $j = 1, ..., N = 3$ thus the Langevin equation in the vector notation, Eq. 4.5, reads

$$\frac{d\vec{y}(t)}{dt} = \vec{q}(t, \vec{y}(t), \langle \vec{\phi} \rangle) + \vec{g}(t, \vec{y}(t), \triangle \vec{\phi}) \cdot \xi(t)$$

where the drift term is $\vec{q} = \{q_1,\ q_2,\ q_3\}$ and the diffusion term is $\vec{g} = \{g_1,\ g_2,\ g_3\}$. We substitute then $\mathrm{L}^* = \langle \mathrm{L}^* \rangle + \triangle \mathrm{L}^* \cdot \xi_\mathrm{L}$ to obtain

$$\begin{aligned}
\frac{\mathrm{dPhy_C}}{\mathrm{dt}} &= \Big(\text{P-R-}(\langle \mathrm{L}^* \rangle + \triangle \mathrm{L}^* \cdot \xi_\mathrm{L}) \cdot \mathrm{Phy_C}\Big) \cdot \mathrm{Phy_C} = \\
&= \underbrace{\big(\text{P-R-}\langle \mathrm{L}^* \rangle \cdot \mathrm{Phy_C}\big) \cdot \mathrm{Phy_C}}_{q_1} \underbrace{\text{-}\triangle \mathrm{L}^* \cdot \mathrm{Phy_C^2}}_{g_1} \cdot \xi_\mathrm{L} \\
\frac{\mathrm{dPhy_N}}{\mathrm{dt}} &= \mathrm{V} \cdot \mathrm{Phy_C} \text{-}(\langle \mathrm{L}^* \rangle + \triangle \mathrm{L}^* \cdot \xi_\mathrm{L}) \cdot \mathrm{Phy_C} \cdot \mathrm{Phy_N} = \\
&= \underbrace{\mathrm{V} \cdot \mathrm{Phy_C} \text{-}\langle \mathrm{L}^* \rangle \cdot \mathrm{Phy_C} \cdot \mathrm{Phy_N}}_{q_2} \underbrace{\text{-}\triangle \mathrm{L}^* \cdot \mathrm{Phy_C} \cdot \mathrm{Phy_N}}_{g_2} \cdot \xi_\mathrm{L}.
\end{aligned}$$

As DIN dynamics does not depend on phytoplankton biomass losses, its equation remains deterministic, thus $q_3 = \frac{\mathrm{dDIN}}{\mathrm{dt}}$ and $g_3 = 0$, and Eq. 4.6 coincides with 4.2. We identify the non null components of the drift term, $\vec{q}$, and the diffusion term, $\vec{g}$, in the two Langevin equations, as defined in 4.5

$$\begin{aligned}
&q_1 = (\text{P-R-}\langle \mathrm{L}^* \rangle) \cdot \mathrm{Phy_C}; && g_1 = -\triangle \mathrm{L}^* \cdot \mathrm{Phy_C^2} \\
&q_2 = \mathrm{V} \cdot \mathrm{Phy_C} \text{-}\langle \mathrm{L}^* \rangle \cdot \mathrm{Phy_C} \cdot \mathrm{Phy_N}; && g_2 = -\triangle \mathrm{L}^* \cdot \mathrm{Phy_C} \cdot \mathrm{Phy_N}.
\end{aligned} \tag{B.5}$$

thus we can apply Eq. 4.6 to solve the state variables dynamics in a intrusive stochastic scheme. Same procedure was applied for the subsistence quota Q^*_{subs}, maximum primary production P_{max} and fraction of protein allocation f_p. Other parameters come non-linearly into the dynamics, thus they uncertainties are not suitable for interpretation in terms of Langevin equations, i.e. it is not possible to recover a form as Eq.4.5 for parameter as size $\ell = \langle \ell \rangle + \triangle \ell \cdot \xi_\ell$.

Bibliography

[Adamson and Morozov, 2014] Adamson, M. and Morozov, A. (2014). Defining and detecting structural sensitivity in biological models: developing a new framework. *Journal of Mathematical Biology*, 69(6-7):1815–1848.

[Aksnes and Egge, 1991] Aksnes, D. L. and Egge, J. K. (1991). A theoretical model for nutrient uptake in phytoplankton. *Marine Ecology Progress Series*, 70:65–72.

[Andersen et al., 2009] Andersen, T., Carstensen, J.and Hernández-Garca, E., and Duarte, C. M. (2009). Ecological thresholds and regime shifts: approaches to identification. *Trends in Ecology and Evolution*, 24(1):49 – 57.

[Antia et al., 1963] Antia, N. J., MacAllistel, C. D., Parsons, T. R., Stephens, K., and Strickland, J. D. H. (1963). Further measurements of primary production using a large-volume plastic sphere. *Limnology and Oceanography*, 8(2):166 – 173.

[Bach et al., 2015] Bach, L. T., Riebesell, U., Gutowska, M. A., Federwisch, L., and Schulz, K. G. (2015). A unifying concept of coccolithophore sensitivity to changing carbonate chemistry embedded in an ecological framework. *Progress in Oceanography*, 135:125 – 138.

[Biddanda and Benner, 1997] Biddanda, B. and Benner, R. (1997). Carbon, nitrogen, and carbohydrate fluxes during the production of particulate and dissolved organic matter by marine phytoplankton. *Limnology and Oceanography*, 42(3):506–518.

[Bonner, 2006] Bonner, J. T. (2006). *Why Size Matters: From Bacteria to Blue Whales*. Princeton University Press.

[Boyce and DiPrima, 2012] Boyce, W. E. and DiPrima, R. C. (2012). *Elementary Differential Equations and Boundary Value Problems*. Wiley, New York, 10 edition.

[Boyd and Gradmann, 2002] Boyd, C. M. and Gradmann, D. (2002). Impact of osmolytes on buoyancy of marine phytoplankton. *Marine Biology*, 141:605–618.

[Broadgate et al., 2013] Broadgate, W., Riebesell, U., Armstrong, C., Brewer, P., Denman, K., Feely, R., Gao, K., Gatusso, J. P., Isensee, K., Kleypas, J., Laffoley, D., Orr, J., Pöetner, H. O., de Rezende, C. E., Schimdt, D., Urban, E., Waite, A., and Valdés, L. (2013). *Ocean acidification summary for policymakers - Third Symposium on the ocean in a high-CO2 world.* International Geosphere-Biosphere Programme, Sweden. p.26.

[Brown et al., 1995] Brown, J. H., Marquet, P. A., and Taper, M. L. (1995). Evolution of body size: consequences of an energetic definition fitness. *The American Naturalist*, 142(4):573–584.

[Brush et al., 2002] Brush, M., Brawley, J., Nixon, S., and Kremer, J. (2002). Modeling phytoplankton production: problems with the Eppley curve and an empirical alternative. *Marine Ecology Progress Series*, 238:31–45.

[Caldeira and Wickett, 2003] Caldeira, K. and Wickett, M. E. (2003). Oceanography: Anthropogenic carbon and ocean ph. *Nature*, 425:365–365.

[Chantrasmi and Iaccarino, 2012] Chantrasmi, T. and Iaccarino, G. (2012). Forward and backward uncertainty propagation for discontinuous system response using the pade-legendre method. *International Journal for Uncertainty Quantification*, 2(2):125–143.

[Chen, 1994] Chen, C. Y. (1994). Effect of ph on the growth and carbon uptake of marine phytoplankton. *Mar. Ecol. Prog. Ser.*, 109:83–94.

[Constantine et al., 2010] Constantine, P. G., Gleich, D. F., and Iaccarino, G. (2010). Spectral methods for parameterized matrix equations. *SIAM Journal on Matrix Analysis and Applications*, 31(5):2681–2699.

[Cornwall and Hurd, 2015] Cornwall, C. E. and Hurd, C. L. (2015). Experimental design in ocean acidification research: problems and solutions. *ICES Journal of Marine Science: Journal du Conseil*.

[Cottingham et al., 2005] Cottingham, K. L., Lennon, J. T., and Brown, B. L. (2005). Knowing when to draw the line: designing more informative ecological experiments. *Frontiers in Ecology and the Environment*.

[Czerny et al., 2013] Czerny, J., Schulz, K. G., Boxhammer, T., Bellerby, R. G. J., Büdenbender, J., Engel, A., Krug, S. A., Ludwig, A., Nachtigall, K., Nondal, G., Niehoff, B., Silyakova, A., and Riebesell, U. (2013). Implications of elevated co2 on pelagic carbon fluxes in an arctic mesocosm study: an elemental mass balance approach. *Biogeosciences*, 10(5):3109–3125.

[Denman and Gargett, 1983] Denman, K. L. and Gargett, A. E. (1983). Time and space scales of vertical mixing and advection of phytoplankton in the upper ocean. *Limnology and Oceanography*, 28(5):801–815.

[Droop, 1973] Droop, M. R. (1973). Some thoughts on nutrient limitation in algae. *Journal of Phycology*, 9(3):264–272.

[Dubinsky et al., 1986] Dubinsky, Z., Falkowski, P. G., and Wyman, K. (1986). Light harvesting and utilization by phytoplankton. *Plant Cell Physiology*, 21(7):1335–134.

[Edwards et al., 2012] Edwards, K., Klausmeier, C. A., and Litchman, E. (2012). Allometric scaling and taxonomic variation in nutrient utilization traits and maximum growth rate of phytoplankton. *Limnology and Oceanography*, 57:554–556.

[Egge et al., 2009] Egge, J. K., Thingstad, T. F. Larsen, A., Engel, A., Wohlers, J., Bellerby, R. G. J., and Riebesell, U. (2009). Primary production during nutrient-induced blooms at elevated co2 concentrations. *Biogeosciences*, 6:877–885.

[Eggers et al., 2014] Eggers, S. L., Lewandowska, A. M., Barcelos e Ramos, J., Blanco-Ameijeiras, S., Gallo, F., and Matthiessen, B. (2014). Community composition has greater impact on the functioning of marine phytoplankton communities than ocean acidification. *Global Change Biology*, 20:713–723.

[Ellison and Williams, 2012] Ellison, S. L. R. and Williams, A. (2012). *Eurachem/CITAC guide: Quantifying Uncertainty in Analytical Measurement*. Third edition. p.26.

[Engel et al., 2014] Engel, A., Cisternas Novoa, C., Wurst, M., Endres, S., Tang, T., Schartau, M., and Lee, C. (2014). No detectable effect of CO2 on elemental stoichiometry of *Emiliania huxleyi* in nutrient-limited, acclimated continuous cultures. *Marine Ecology Progress Series*, 507:15–30.

[Engel et al., 2005] Engel, A. et al. (2005). Testing the direct effect of CO2 concentration on a bloom of the coccolithophorid *Emiliania huxleyi* in mesocosm experiments. *Limnology and Oceanography*, 50(2):493–507.

[Engel et al., 2008] Engel, A., Schulz, K. G., Riebesell, U., Bellerby, R., Delille, B., and Schartau, S. (2008). Effects of CO2 on particle size distribution and phytoplankton abundance during a mesocosm bloom experiment (PeECE II). *Biogeosciences*, 5:509–521.

[Eppley, 1972] Eppley, R. W. (1972). Temperature and phytoplankton growth in the sea. *Fishery Bulletin*.

[Field et al., 2008] Field, A., Miles, J., and Field, Z. (2008). *Discovering statistics using R*. SAGE Publications Ltd.

[Gattuso et al., 2011] Gattuso, J. P., Bijma, J., Gehlen, M., Riebesell, U., and Turley, C. (2011). Effects of ocean acidification on pelagic organisms and ecosystems. In Gattuso, J. P. and Hansson, L., editors, *Ocean Acidification*, pages 291–311. Oxford University Press.

[Geider et al., 1998a] Geider, R., Macintyre, Graziano, L., and McKay, R. M. (1998a). Responses of the photosynthetic apparatus of *dunaliella tertiolecta* (chlorophyceae) to nitrogen and phosphorus limitation. *European Journal of Phycology*, 33(4):315–332.

[Geider et al., 1998b] Geider, R. J., Maclntyre, H. L., and Kana, T. M. (1998b). A dynamic reg-

ulatory model of phytoplanktonic acclimation to light, nutrients, and temperature. *Limnology and Oceanography*, 43(4):679–694.

[Ghanem and Spanos, 1991] Ghanem, R. G. and Spanos, P. D. (1991). *Stochastic Finite Elements: A Spectral Approach*. Springer-Verlag New York, Inc. New York, NY, USA.

[Hönisch et al., 2012] Hönisch, B., Ridgwell, A., Schmidt, D. N., Thomas, E., Gibbs, S. J., Sluijs, A., Zeebe, R., Kump, L., Martindale, R. C., Greene, S. E., Kiessling, W., Ries, J., Zachos, J. C., Royer, D. L., Barker, S., Marchitto, T. M., Moyer, R., Pelejero, C., Ziveri, P., Foster, G. L., and Williams, B. (2012). The geological record of ocean acidification. *Science*, 335(6072):1058–1063.

[Horn et al., 2015] Horn, H. G., Boersma, M., Garzke, J., Lder, M. G. J., Sommer, U., and Aberle, N. (2015). Effects of high co2 and warming on a baltic sea microzooplankton community. *ICES Journal of Marine Science: Journal du Conseil*.

[Jones et al., 2014] Jones, B. M., Iglesias-Rodriguez, M. D., Skipp, P. J., Edwards, R. J., Greaves, M. J., et al. (2014). Responses of the *Emiliania huxleyi Proteome* to Ocean Acidification. *PLoS ONE*, 8(4):2857–2869.

[Kennedy and O'Hagan, 2001] Kennedy, M. C. and O'Hagan, A. (2001). Bayesian calibration of computer models. *Journal of the Royal Statistical Society, Series B*, 63:425–464.

[Kim et al., 2006] Kim, J.-M., Lee, K., Shin, K., Kang, J.-H., Lee, H.-W., Kim, M., Jang, P.-G., and Jang, M.-C. (2006). The effect of seawater CO2 concentration on growth of a natural phytoplankton assemblage in a controlled mesocosm experiment. *Limnology and Oceanography*, 51(4):1629–1636.

[Klepper, 1997] Klepper, O. (1997). Multivariate aspects of model uncertainty analysis: tools for sensitivity analysis and calibration. *Ecological Modelling*, 101(1):1 – 13.

[Kroeker et al., 2013] Kroeker, K. J., Kordas, R. L., Crim, R., Hendriks, I. E., Ramajo, L., Singh, G. S., Duarte, C. M., and Gattuso, J.-P. (2013). Impacts of ocean acidification on marine organisms: quantifying sensitivities and interaction with warming. *Global Change Biology*, 19(6):1884–1896.

[Larssen et al., 2006] Larssen, T., Huseby, R. B., Cosby, B. J., Høst, G., Høgåsen, T., and Aldrin, M. (2006). Forecasting acidification effects using a bayesian calibration and uncertainty propagation approach. *Environmental Science Technology*, 40.

[Ley and Mauzerall, 1982] Ley, A. C. and Mauzerall, D. C. (1982). Absolute absorption cross-sections for photosystem II and the minmum quantum requirement for photosynthesis in chlorella vulgaris. *Biochimica et Biophysica Acta*, 680:95–106.

[Litchman et al., 2010] Litchman, E., de Tezanos-Pinto, P., Klausmeier, C. A., Thomas, M. K., and Yoshiyama, K. (2010). Linking traits to species diversity and community structure in phytoplankton. *Hydrobiologia*, 653(1):15–28.

[Litchman et al., 2007] Litchman, E., Klausmeier, C. A., Schofield, O., and Falkowski, P. (2007). The role of functional traits and trade-offs in structuring phytoplankton communities: scaling from cellular to ecosystem level. *Ecology Letters*, 10:1170–1181.

[Litchman et al., 2009] Litchman, E., Klausmeier, C. A., and Yoshiyama, K. (2009). Contrasting size evolution in marine and freshwater diatoms. 106(8):2665–2670.

[Litchman and Klausmeier, 2008] Litchman, L. and Klausmeier, C. A. (2008). Trait-Based Community Ecology of Phytoplankton. *The Annual Review of Ecology, Evolution, and Systematics*, 39:615–639.

[Marbà et al., 2007] Marbà, N., Duarte, C. M., and Agustí, S. (2007). Allometric scaling of plant life history. *Proceedings of the National Academy of Sciences*, 104(40):15777–15780.

[Miller, 1988] Miller, R. G. J. (1988). *Beyond ANOVA, Basics of Applied Statistics*. Wiley, New York - Chichester - Brisbane - Toronto - Singapore.

[Montagnes and Lessard, 1999] Montagnes, D. J. S. and Lessard, E. J. (1999). Population dynamics of the marine planktonic ciliate *strombidinopsis multiauris*: its potential to control phytoplankton blooms. *Aquat. Microb. Ecol.*, 20:167–181.

[Pahlow, 2005] Pahlow, M. (2005). Linking chlorophyllnutrient dynamics to the Redfield N:C ratio with a model of optimal phytoplankton growth. *Marine Ecology Progress Series*, 287:33–43.

[Pahlow and Oschlies, 2013] Pahlow, M. and Oschlies, A. (2013). Optimal allocation backs Droops cell-quota model. *Marine Ecology Progress Series*, 473:1–5.

[Paul et al., 2015] Paul, C., Matthiessen, B., and Sommer, U. (2015). Warming, but not enhanced CO2 concentration, quantitatively and qualitatively affects phytoplankton biomass. *Marine Ecology Progress Series*, 528:39–51.

[Peterman, 1990] Peterman, R. M. (1990). The importance of reporting statistical power: the forest decline and acidic deposition example. *Ecology*, 71(5):2024–2027.

[Peters, 1983] Peters, R. H. (1983). *The Ecological Implications of Body Size*. Cambridge University Press. Cambridge Books Online.

[Raven and Beardall, 2003] Raven, J. and Beardall, J. (2003). Carbon acquisition mechanisms of algae: Carbon dioxide diffusion and carbon dioxide concentrating mechanisms. In Larkum, A., Douglas, S., and Raven, J., editors, *Photosynthesis in Algae*, volume 14 of *Advances in Photosynthesis and Respiration*, pages 225–244. Springer Netherlands.

[Raven, 1980] Raven, J. A. (1980). Nutrient transport in microalgae. *Adv. Microb. Physiol.*, 21:47–226.

[Ridgwell et al., 2009] Ridgwell, A., Schmidt, D. N., Turley, C., Brownlee, C., Maldonado, M. T., Tortell, P., and Young, J. R. (2009). Past constraints on the vulnerability of marine calcifiers

to massive carbon dioxide release. *Nature Geosci*, 3:196–200.

[Riebesell et al., 2008] Riebesell, U., Bellerby, R. G. J., Grossart, H. P., and Thingstad, F. (2008). Mesocosm co2 perturbation studies: from organism to community level. *Biogeosciences*, 5:1157–1164.

[Riebesell et al., 2010] Riebesell, U., Fabry, V. J., Hansson, L., and Gattuso, J. P. (2010). *Guide to best practices for ocean acidification research and data reporting*. Publications Office of the European Union.

[Riebesell et al., 2007] Riebesell, U., Schulz, K. G., Bellerby, R. G. J., Botros, M., Fritsche, P., Meyerhofer, M., Neill, C., Nondal, G., Oschlies, A., Wohlers, J., and Zollner, E. (2007). Enhanced biological carbon consumption in a high co2 ocean. *Nature*, 450:545–548.

[Riebesell et al., 1993] Riebesell, U., Wolf-Gladrow, D. A., and Smetacek, V. (1993). Carbon dioxide limitation of marine phytoplankton growth rates. *Nature*, 361:249–251.

[Riebesell et al., 2000] Riebesell, U., Zondervan, I., Rost, B., Tortell, P. D., Zeebe, R. E., and Morel, F. M. M. (2000). Reduced calcification of marine plankton in response to increased atmospheric. *Nature*, 407:364–367.

[Rose, 2007] Rose, J. M., D. A. C. (2007). Does low temperature constrain the growth rates of heterotrophic protists? evidence and implications for algal blooms in cold waters. *Limnology and Oceanography*, 52:37–46.

[Rost et al., 2003] Rost, B., Riebesell, U., Burkhardt, S., and Sueltemeyer, D. (2003). Carbon acquisition of bloom-forming marine phytoplankton. *Limnology and Oceanography*, 48(1):55–67.

[Ruxton and Colegrave, 2006] Ruxton, G. D. and Colegrave, N. (2006). *Experimental design for the life sciences*. Oxford: Oxford University Press.

[Sabine et al., 2004] Sabine, C. L., Feely, R. A., Gruber, N., Key, R. M., Lee, K., Bullister, J. L., Wanninkhof, R., Wong, C. S., Wallace, D. W. R., Tilbrook, B., Millero, F. J., Peng, T.-H., Kozyr, A., Ono, T., and Rios, A. F. (2004). The Oceanic Sink for Anthropogenic CO2. *Science*, 305(5682):367–371.

[Scalley and Baker, 1997] Scalley, M. L. and Baker, D. (1997). Protein folding kinetics exhibit an arrhenius temperature dependence when corrected for the temperature dependence of protein stability. *Proceedings of the National Academy of Sciences*, 94(20):10636–10640.

[Schartau et al., 2007] Schartau, M., Engel, A., Schröter, J., Thoms, S., Völker, C., and Wolf-Gladrow, D. (2007). Modelling carbon overconsumption and the formation of extracellular particulate organic carbon. *Biogeosciences*, 4(4):433–454.

[Schluter et al., 2014] Schluter, L., Lohbeck, K. T., Gutowska, M. A., Groger, J. A., Riebesell, U., and Reusch, T. B. H. (2014). Adaptation of a globally important coccolithophore to ocean

warming and acidification. *Nature Climate Change*, 4:1024–1030.

[Schulz et al., 2008] Schulz, K. G., Riebesell, U., Bellerby, R. G. J., Biswas, H., Meyerhöfer, M., Müller, M. N., Egge, J. K., Nejstgaard, J. C., Neill, C., Wohlers, J., and Zöllner, E. (2008). Build-up and decline of organic matter during peece iii. *Biogeosciences*, 5:707–718.

[Sommer et al., 2015] Sommer, U., Paul, C., and Moustaka-Gouni, M. (2015). Warming and Ocean Acidification Effects on Phytoplankton - From Species Shifts to Size Shifts within Species in a Mesocosm Experiment. *PLOS ONE*, 10:39–51.

[Strogatz, 2014] Strogatz, S. H. (2014). *Nonlinear Dynamics and Chaos with applications to physics, biology, chemistry and engineering.* Westview Press.

[Suzuki and Takahashi, 1995] Suzuki, Y. and Takahashi, M. (1995). Growth responses of several diatom species isolated from various environment temperature. *Journal of Phycology*, 31(6):880–888.

[Tanaka et al., 2008] Tanaka, T., Thingstad, T. F., Løvdal, T., Grossart, H.-P., Larsen, A., Allgaier, M., Meyerhöfer, M., Schulz, K. G., Wohlers, J., Zöllner, E., and Riebesell, U. (2008). Availability of phosphate for phytoplankton and bacteria and of glucose for bacteria at different pco_2 levels in a mesocosm study. *Biogeosciences*, 5(3):669–678.

[Toral and Colet, 2014] Toral, R. and Colet, P. (2014). *Stochastic Numerical Methods.* Wiley-VCH.

[Tortell et al., 2008] Tortell, P. D., Payne, C. D., Li, Y., Trimborn, S., Rost, B., Smith, W. O., Riesselman, C., Dunbar, R. B., Sedwick, P., and DiTullio, G. R. (2008). Co2 sensitivity of southern ocean phytoplankton. *Geophysical Research Letters*, 35(4):n/a–n/a. L04605.

[Weisse and Montagnes,] Weisse, J. and Montagnes, M. Effect of temperature on inter- and intraspecific isolates of *urotricha* (prostomatida, ciliophora).

[Wirtz, 2011] Wirtz, K. W. (2011). Non-uniform scaling in phytoplankton growth rate due to intracellular light and CO_2 decline. *Journal of Plankton Research*, 33(9):1325–1341.

[Wirtz, 2013] Wirtz, K. W. (2013). Mechanistic origins of variability in phytoplankton dynamics: Part I: Niche formation revealed by a Size-Based Model. *Marine Biology.*

[Wirtz and Eckhardt, 1996] Wirtz, K. W. and Eckhardt, B. (1996). Effective variables in ecosystem models with an application to phytoplankton succession. *Ecological Modelling*, 92(1):33–53.

[Wirtz and Pahlow, 2010] Wirtz, K. W. and Pahlow, M. (2010). Dynamic chlorophyll and nitrogen:carbon regulation in algae optimizes instantaneous growth rate. *Marine Ecology Progress Series*, 402:81–9.

[Zondervan et al., 2001] Zondervan, I., Zeebe, R. E., Rost, B., and Riebesell, U. (2001). Decreasing marine biogenic calcification: A negative feedback on rising atmospheric pco2. *Global*

Biogeochemical Cycles, 15(2):507–516.